Eur. Phys. J. D **19**, 193–209 (2002)
DOI: 10.1140/epjd/e20020071

THE EUROPEAN PHYSICAL JOURNAL D
EDP Sciences

Ultrafast dynamics in the excited hydrogen atom transfer states of ammonia clusters*

Size dependent photoelectron spectroscopy in a three color femtosecond pump-control-probe experiment

P. Farmanara[1], H.-H. Ritze[1], V. Stert[1], W. Radloff[1,a], and I.V. Hertel[1,2,b]

[1] Max-Born-Institut für Nichtlineare Optik und Kurzzeitspektroskopie, Max-Born-Str. 2A, 12489 Berlin-Adlershof, Germany
[2] Fachbereich Physik, Freie Universität Berlin, Arnimallee 14, 14195 Berlin, Germany

Received 22 September 2001 and Received in final form 31 January 2002

Abstract. Neutral ammonia clusters $(NH_3)_m$ are photo-excited to the electronic $\tilde{A}$ state by a deep UV femtosecond laser pump pulse. Within a few hundred femtoseconds a significant fraction of the clusters rearrange to form an *H-transfer state* $(NH_3)_{m-2}NH_4(3s)NH_2$ with the subunit NH_4 in its $3s$ electronic ground state. This state is then electronically excited by a time-delayed infrared control pulse of variable wavelength. Finally, a third (probe) pulse in the UV ionizes the clusters for detection. The lifetime of the excited $(NH_3)_{m-2}NH_4(3p)NH_2$ states is found to vary between 2.7 and 0.13 ps depending on cluster size and excitation energy. It increases drastically upon deuteration. The corresponding cluster size-dependent photoelectron spectra allow us to disentangle the underlying energetics of the excitation and ionization process and reveal additional processes, such as nonresonant ionization or dissociative ionization. The experimental findings suggest that the excited H-transfer ammonia complexes with $m > 2$ are deactivated by an internal conversion process back to the electronically lowest H-transfer state followed by fast dissociation.

PACS. 36.40.Mr Spectroscopy and geometrical structure of clusters – 36.40.Sx Diffusion and dynamics of clusters – 42.65.Re Ultrafast processes; optical pulse generation and pulse compression – 33.60.-q Photoelectron spectra – 82.30.Nr Association, addition, insertion, cluster formation

1 Introduction

For a long time, ammonia clusters have attracted the interest of researchers in physics and chemistry as prototype complexes of polar molecules allowing for a variety of elementary key processes to be studied. Understanding the kinetics and dynamics of the internal hydrogen and proton transfer is of fundamental importance for many chemical reactions and has been studied in detail theoretically (see *e.g.* [1–7]) as well as experimentally (*e.g.* [8–15]). In most experiments, clusters are ionized by one or several photons and are subsequently mass selected before detection. Typical mass spectra of ammonia clusters are dominated by protonated ions $(NH_3)_{m-2}NH_4^+$ while the signals with a mass corresponding to $(NH_3)_m^+$ are very weak. It is now understood that vertical transitions from the weakly bound ground state of the neutral clusters lead to an ionic geometry where one of the ammonia molecules is in a vibrationally excited state of the NH_3^+ ion (its ground state configuration being planar) while the other constituents remain unexcited, essentially in their original pyramidal NH_3 geometry, as schematically illustrated in Figure 1.

We call these ionic configurations $(NH_3)_{m-2}NH_3^+ ...NH_3$ the *adiabatic monomer in dimer, trimer (AMD, AMT)* etc. states. Their energies lie far above the energetically most stable ionic configurations $(NH_3)_{m-2}NH_4^+ ...NH_2$, the so-called *internally protonated monomer in dimer, trimer (PMD, PMT)* etc. state. The latter cannot be reached directly *via* Franck-Condon transitions from the neutral ground states as obvious from the left upper panel of Figure 1. Hence, in ionization experiments typically much of the vibrational energy is initially stored in the cluster ions. After geometrical rearrangement of the *AMD, AMT...* states to the *PMD, PMT...* configuration

$$(NH_3)_{m-2}NH_3^+ ...NH_3 \rightarrow (NH_3)_{m-2}NH_4^+ ...NH_2$$

this leads finally to stabilization by NH_2 ejection and formation of protonated cluster ions:

$$(NH_3)_{m-2}NH_4^+ ...NH_2 \xrightarrow{-NH_2} (NH_3)_{m-2}NH_4^+ .$$

* Figures are available in color at: http://www.edpsciences.org/epjd/

[a] e-mail: radloff@mbi-berlin.de
[b] e-mail: hertel@mbi-berlin.de

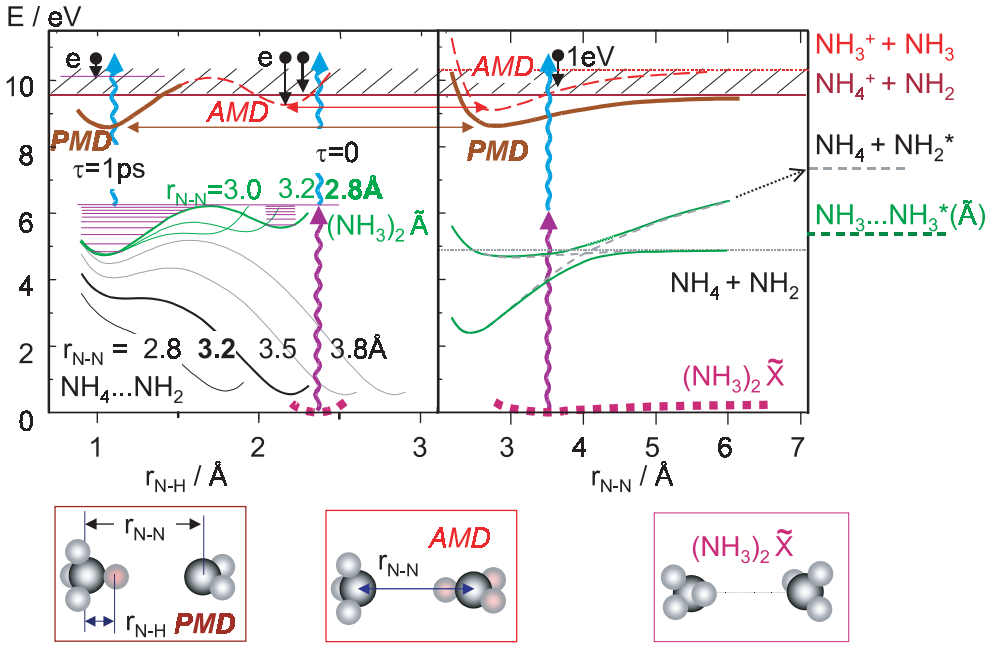

Fig. 1. Schematic of the potential energies (upper panels) and geometry (lower panels) for ground, excited and ionic state of the ammonia dimer. Shown are two cuts through the potential energy surface along the H–N and N–N coordinate, respectively. The energetically lowest ionic state is the *protonated monomer in dimer (PMD)* while in a fast ionization process the *adiabatic monomer in dimer (AMD)* is reached. The excited state has a similar geometry. Also indicated (on the left side) is a potential scheme for accessing the *PMD* state in an experiment with a delayed probe photon.

Finally, after a (possibly metastable) loss of NH_3 (and hence cooling of the cluster), the characteristic mass spectrum is formed.

The present work is dedicated to a detailed study of the neutral equivalent of these processes, in particular to the dynamics of the excited H-transfer states which can be selectively populated by suitable femtosecond laser pulses. Femtosecond (fs) pump-probe spectroscopy has in the past proved to be a powerful tool for the study of unimolecular rearrangement and dissociation processes of gas phase molecular systems. Previous real time measurements of neutral ammonia clusters with femtosecond pump-probe techniques in the UV [16–22,24–28,31] and VUV [23] spectral range have lead to an understanding of the basic mechanisms involved in the excited state dynamics: a thorough analysis [21] of the pump-probe signals has revealed that within $\sim 180...270$ fs (depending on cluster size) after excitation to their first electronically excited $\tilde{A}$ state the clusters decay, but partially also rearrange internally within the excited state. This geometry change on the $\tilde{A}$ state potential energy surface

$$(NH_3)_{m-2}NH_3(\tilde{A})...NH_3 \rightarrow (NH_3)_{m-2}NH_4(3s)...NH_2$$

leads to a *hydrogen atom transfer state* $(NH_3)_{m-2}NH_4...NH_2$ (*cf.* Fig. 1). This state, as the proton transfer state of the cluster ions, has a lower energetic minimum than the initially excited configuration with a well depth of about 1 to 1.5 eV [7]. Again, for Franck-Condon reasons it cannot be populated directly from the electronic ground state and is much more stable than the initially excited $\tilde{A}$ state, its lifetime being a few picoseconds. Thus we may call it a bound state on the fs time scale. As we have shown in earlier work (in particular for the ammonia dimer [28]) it is possible to purposefully modify the reaction kinetics of the cluster ions by a judiciously chosen fs *control pulse* in the near infrared. The latter transfers excess energy from vibrational into electronic degrees of freedom within the neutral precursors of the ammonia cluster ions, which are finally created by a *probe pulse* prior to mass resolved detection. As the experiments have shown in this manner a massive reduction of protonated species may be induced by the *control pulse*.

In the present work such a fs-near-IR pulse of variable wavelength will be used to investigate the dynamics of the ground and excited state *hydrogen atom transfer configuration* as a function of cluster size. In view of the previous studies we keep the terminology *pump-probe-control experiment*, although in the present work the emphasis is on spectroscopy rather than on control.

A kinetic model describing the earlier *"simple" pump-probe* experiments has been discussed and verified in great detail in previous publications (see *e.g.* [22]). A careful analysis of the experimental data within this now well established kinetic model is a prerequisite for understanding the modified dynamics and spectroscopy which may be revealed when the additional *control* photon is applied, in particular for clusters larger than the ammonia dimer which are the main focus of the present work. As in one-photon ionization experiments, due to excess energy after ionization the mass spectra in the two photon studies show strong $(NH_3)_{m-2}NH_4^+$ and much weaker $(NH_3)_m^+$ cluster ion signals. In addition to the H-atom

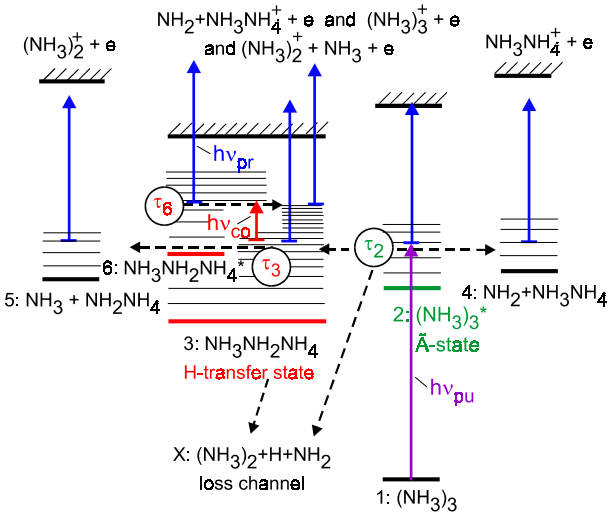

Fig. 2. Kinetic model for the photoinduced dynamics in ammonia clusters, demonstrated, as an example, for the trimer. The H-atom transfer state (3), populated *via* the optically accessible $\tilde{A}$ state (2) and therefore highly vibrationally excited, is further excited by a time-delayed photon (∼1 ps) to its higher electronic states (6). The corresponding lifetimes τ_2, τ_3 and τ_6 can be revealed by scanning the probe pulse.

migration dynamics other decay channels, such as NH_2 loss, are open for the initially excited $\tilde{A}$ state levels, thus reducing the signal arising from so-called *ADI (absorption dissociation ionization) processes* [16,17]. In addition, *AID processes (absorption ionization dissociation)* can occur, *i.e.* ionization of intact excited neutral clusters with subsequent stabilization by NH_2 ejection or NH_3 evaporation in the ionic system. The different channels involved are illustrated very schematically in Figure 2 also indicating the additional role of the control photon.

The interpretation of the experimental results is further facilitated by the results of *ab initio* calculations [25] which we have performed for the ammonia dimer in the vicinity of the equilibrium configurations of both, the H- and the proton-transfer states. Because of their similarity only minor changes of the vibrational energy can be induced by Franck-Condon transitions between these states. By employing femtosecond time-resolved photoelectron spectroscopy *FEICO (Femtosecond Electron Ion Coincidence)* [24–26] we were able to confirm the theoretical predictions *e.g.* for the minimum potential energy of the H- and the proton-transfer states, being 4.74 eV and 8.62 eV, respectively. Recently, we have extended these calculations and measurements to the first few electronically excited states of the dimer and trimer [27,28]. Experimentally, excitation of the ammonia clusters from the H-transfer configuration – populated by internal rearrangement after the initial photo-excitation with the pump pulse at about 200 nm – to higher electronic states was accomplished by an infrared laser *control*–pulse at 832 nm, 1 200 nm or 1 400 nm, suitably delayed in time with respect to the UV pump pulse. Because the clusters exist for a few ps in the H-transfer state while the initially excited $\tilde{A}$ state decays with time constants of about 180...270 fs we have chosen delay times between 1 and 2 ps so that the observed three color signals arise mostly from the H-transfer state. Detection of the clusters was finally achieved by a third femtosecond pulse, the probe pulse, at about 400 nm whose delay is varied. Although the energetics – determined by *ab initio* calculations and verified by photoelectron spectroscopy – turns out to be rather similar for the ammonia dimer and trimer, the time-dependent ion signals reveal a completely different dynamical behavior. While the trimer lifetime strongly depends on the infrared control photon energy and on the H (D) isotopes studied, the dimer signal decays at about the same rate at all experimental conditions. Obviously, different decay mechanisms are responsible for this astonishing difference between dimer and trimer.

It is one of the main goals of the present work to provide a satisfactory explanation for this behavior by a systematic study of time-dependent ion signals and photoelectron spectra *(PES)* for larger ammonia clusters. To this end we also study their deuterated counterparts and compare the dynamics for different infrared control pulse wavelengths.

2 Experimental setup and procedure

A detailed description of the experimental setup has been given in previous publications [21,31]. Briefly, the clusters are generated and cooled by adiabatic expansion of ammonia (about 10%) seeded in He gas (1.2 bar) through a pulsed nozzle. We use undeuterated NH_3 as well as fully deuterated ND_3 ammonia gas. While our previous studies focussed essentially on the ammonia dimer [24,25] and to some extent also on the trimer [27,28] and hence the fraction of higher clusters present in the cluster beam was minimized, the present study concentrates on larger ammonia clusters and we use a high stagnation pressure in the molecular beam expansion leading to a broad cluster distribution. After passing a skimmer (diam. 1 mm), the molecular beam reaches the ionization region of a Wiley-McLaren TOF mass spectrometer where the ammonia clusters interact with the femtosecond laser pulses of three mildly focused co-propagating laser beams. In two sets of experiments the clusters are excited into their $\tilde{A}$ state by a pump pulse at $\lambda_{pu} = 208$ nm $\widehat{=}$ 5.96 eV (alternatively 200 nm $\widehat{=}$ 6.2 eV) and ionized by a probe pulse at $\lambda_{pr} = 416$ nm $\widehat{=}$ 2.98 eV (alternatively 400 nm $\widehat{=}$ 3.1 eV). The time-delay τ of the latter can be scanned with respect to the pump pulse by a standard delay line. An additional pulse, the *control pulse* at $\lambda_{co}^{(1)} = 832$ nm $\widehat{=}$ 1.49 eV, $\lambda_{co}^{(2)} = 1\,200$ nm $\widehat{=}$ 1.03 eV or $\lambda_{co}^{(3)} = 1\,400$ nm $\widehat{=}$ 0.89 eV is delayed by a fixed time (typically $\tau_{co} = 1.2$ ps) with respect to the pump pulse, using a second delay line. The sum of photon energies $h\nu_{pu} + h\nu_{pr} + h\nu_{co}$ must be kept at a low enough level above the appearance potential for the protonated clusters (9.54, 9.13 and 9.11 eV for the dimer, trimer and tetramer, respectively [13]) in order to

detect a significant ion signal from the homogeneous clusters $(NH_3)_m^+$ in the three-color experiments.

In the first set of experiments we therefore use the red edge of the Ti:sapphire laser tuning range ($\lambda_{pu} = 208$ nm, $\lambda_{pr} = 416$ nm, $\lambda_{co}^{(1)} = 832$ nm as in [28]), the total photon energy being 10.43 eV. We restrict the experiments to comparatively low laser fluences so that competitive ionization channels due to resonance-enhanced one- and two-color multiphoton ionization ($h\nu_{pu} + h\nu_{pu}$, $h\nu_{pu} + 2h\nu_{pr}$, $h\nu_{pu} + 3h\nu_{co}$) can be neglected, thus avoiding the three-color signal to be obstructed by a significant background. This also reduces fragmentation within the ionic system, *i.e.* the contribution of larger cluster ions $(NH_3)_{m+1}^+$ and $(NH_3)_{m+2}^+$ to the dominant protonated species $(NH_3)_{m-2}NH_4^+$. These arise from fragmentation of vibrationally hot unprotonated ions

$$(NH_3)_m^+(\text{hot}) \rightarrow (NH_3)_{m-2}NH_4^+ + NH_2.$$

Low excess energy reduces the subsequent NH_3 evaporation (once or twice) according to the scheme:

$$\begin{array}{ccccc} (NH_3)_m NH_4^+ & \xrightarrow{-NH_3} & (NH_3)_{m-1}NH_4^+ & \xrightarrow{-NH_3} & (NH_3)_{m-2}NH_4^+ \\ {\scriptstyle -NH_2}\nearrow & & {\scriptstyle -NH_2}\nearrow & & {\scriptstyle -NH_2}\nearrow \\ (NH_3)_{m+2}^+ & \xrightarrow{-NH_3} & (NH_3)_{m+1}^+ & \xrightarrow{-NH_3} & (NH_3)_m^+ \end{array}$$

In the second set of experiments we use $\lambda_{co}^{(2)} = 1\,200$ nm or $\lambda_{co}^{(3)} = 1\,400$ nm as control pulse wavelengths so that the pump and probe wavelengths can be chosen as in our earlier experiments [19,21,22,24–27,31] ($\lambda_{pu} = 200$ nm and $\lambda_{pr} = 400$ nm) giving an even lower total photon energy (10.33 eV or 10.19 eV, respectively) – and hence further reduced fragmentation of larger cluster ions.

Time-resolved photoelectron-photoion coincidence spectra are obtained by detecting the ions with a TOF mass spectrometer while the corresponding photoelectrons are analyzed by a time-of-flight magnetic bottle electron spectrometer. The ion and electron signals obtained *via* microchannel plate detectors are amplified and then fed into the entrance channels of a two-channel multi-hit time-to-digital converter TDC (Le Croy model 4208) triggered by the laser pulses with a repetition rate of 1 kHz. This allows us to derive photoelectron spectra (PES) for each cluster and its fragments individually. In contrast, when recording only the time-dependent ion signals without photoelectron detection the output of the microchannel plates is digitized by a fast digital oscilloscope (Tektronix TDS 540) and then stored and processed by a PC. Typically, the mass spectra obtained here are added for 100 laser pulses at each delay time with a pulse repetition rate of 70 Hz and averaged over 30 back and forth delay scans.

In the first set of experiments a regenerative amplifier (Quantronix Model 4810/20) is used, seeded by an Ar-ion laser pumped Ti:sapphire laser (Spectra Physics TSUNAMI) tuned to $\lambda = 832$ nm. The pulse energy is 0.5 mJ. In the second set of experiments we use a diode-pumped Ti:sapphire laser and regenerative amplifier system (Clark MXR) at $\lambda = 800$ nm in combination with

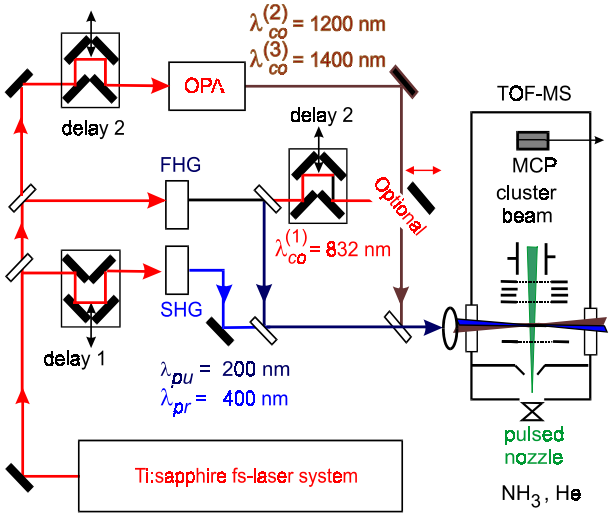

Fig. 3. Schematic of the experimental set-up used in the three-color experiments. The *control* pulse wavelength is tuned by choosing either a fraction of the fundamental beam ($\lambda_{co}^{(1)} = 832$ nm) or the output from the OPA ($\lambda_{co}^{(2,3)} = 1\,200$ or $1\,400$ nm). In the former case we have $\lambda_{pu} = 208$ nm and $\lambda_{pr} = 416$ nm, while in the latter case we tune the Ti:sapphire laser to 800 nm so that $\lambda_{pu} = 200$ nm and $\lambda_{pr} = 400$ nm. The time-delays τ_{pr} and τ_{co} of probe and control pulse relative to the pump pulse can be adjusted individually (delay 1 and delay 2). Typically, τ_{co} is kept constant at 1.2 ps. For measuring time dependent ion signals τ_{pr} is scanned while for recording the photoelectron spectra (PES) it is set to $\tau_{pr} = 1.3$ ps.

a commercial OPA system (Clark I-GOR-SHG). In Figure 3 the subsequent frequency conversion stages are indicated for both cases. The amplified laser beam is split into two (three) parts, one of which is transformed to the fourth harmonic by three successive BBO crystals [29] and is used as pump pulse. The second part of the laser beam is frequency doubled by an additional BBO crystal and serves as probe pulse. In the first set of experiments ($\lambda_{co}^{(1)} = 832$ nm) we use the residual part of the fundamental wave which has not been converted during the sum frequency generation of the fourth harmonic as control pulse. For the second set of experiments we use the OPA output at $\lambda_{co}^{(2)} = 1\,200$ nm or $\lambda_{co}^{(3)} = 1\,400$ nm. The temporal width τ_L (FWHM) of the laser pulses is about 200 fs for the Spectra/Quantronix system and about 130 fs for the Clark MXR. It is continuously monitored online for the fundamental wave (and optimized if necessary) using an autocorrelator or a FROG. Typically, the fluences of the laser beams are kept at a low fluence (see above) of about 0.05 mJ/cm^2 for the pump pulse, 1 mJ/cm^2 for the probe pulse and 4 mJ/cm^2 and 20 mJ/cm^2 for a control pulse of $\lambda_{co}^{(1)} = 832$ nm and $\lambda_{co}^{(2)} = 1\,200$ nm (or $\lambda_{co}^{(3)} = 1\,400$ nm), respectively. For the coincidence detection of photoions and photoelectrons a low ionization rate has to be ensured in order to suppress accidental coincidences. In our experiments an average of about 1 ion is detected per 20 laser pulses. This low rate is due to the low laser fluences and the fact that the final two-color, two photon ionization

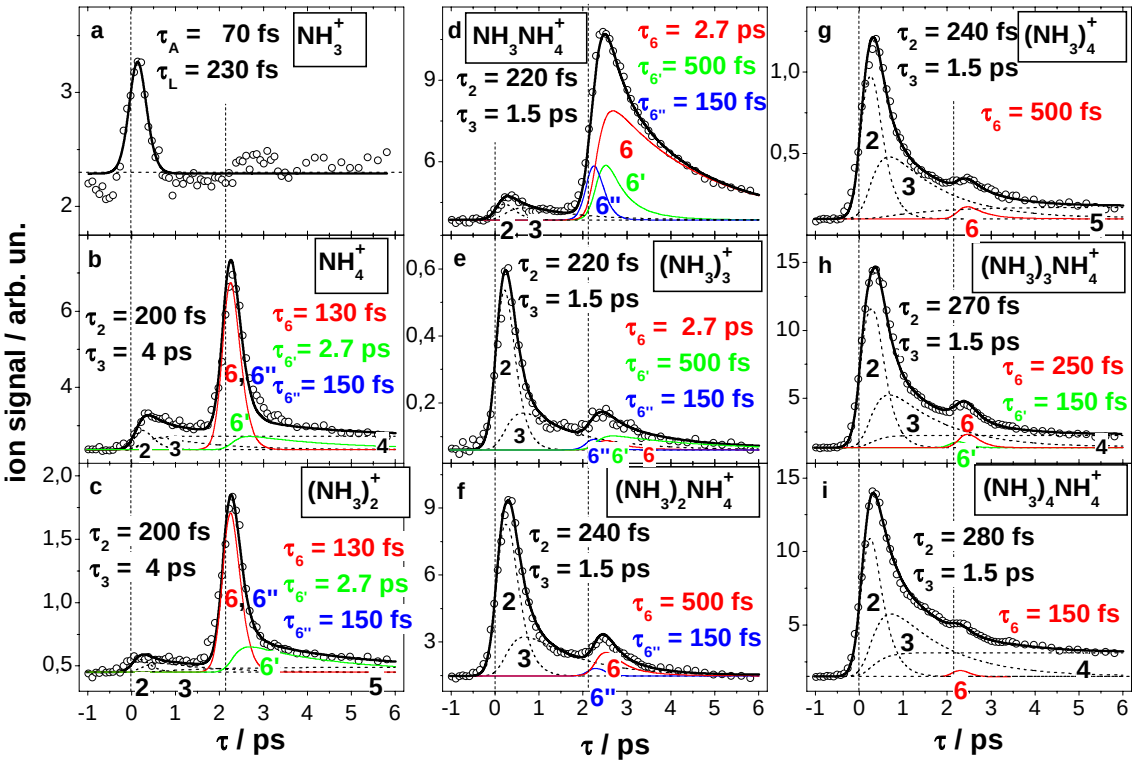

Fig. 4. Ion yield of $(NH_3)_m^+$ (m = 1, 2, 3, 4 in panel a, c, e, g, respectively) and $(NH_3)_{m-2}NH_4^+$ (m = 2...6 in b, d, f, h, i, respectively) as a function of the delay time between pump (λ_{pu} = 208 nm) and probe pulse (λ_{pr} = 416 nm). The control pulse ($\lambda_{co}^{(1)}$ = 832 nm) is delayed by 2.1 ps with respect to the pump. The heavy line represents the fit according to our kinetic model (Fig. 2). It contains the contributions from the two-color signal (dashed lines 2, 3, 4, 5) as well as that from the H-transfer state (6) (thin solid line), electronically excited by the control pulse. (6′, 6″) is due to dissociative ionization as explained in the text. The relaxation times τ_i of the different channels as derived from the fit are also indicated (for the two-color signals we use the values from Ref. [22]).

process can act only on those clusters which have survived in the H-transfer state for 1.2 ps after excitation by the initial pump pulse. At such low count rates the contribution of uncorrelated coincidences is below 10% and can be neglected. On the other hand, the low coincidence rate requires at a pulse repetition frequency of 1 kHz and a data acquisition time of at least 1 h to accumulate about 2×10^5 coincidences.

3 Experimental results

3.1 Control pulse wavelength 832 nm

In Figures 4 and 5 the time-dependent ion signals are shown for $(NH_3)_m$ and $(ND_3)_m$ clusters, respectively. The data points represent the total signals consisting of the usual two-color pump-probe signals and the superimposed *three-color signals*. It is obvious that the control pulse ($\lambda_{co}^{(1)}$ = 832 nm) applied 2.1 (or 1.7) ps after the pump pulse (λ_{pu} = 208 nm) induces a new dynamics as revealed by scanning the delay time of the probe pulse (λ_{pr} = 416 nm). The dashed lines represent the two-color pump-probe signals fitted by our standard procedure [21] using time constants identical to those derived in [22]. The three-color ion signals are fitted by a completely analogous procedure (thin solid lines) which allows us to extract contributions from the different processes discussed in detail in the next section. The superposition of all contributions results in the total signals drawn as heavy solid lines. The zero delay time between control and probe pulse is calibrated most reliably by using the fits to the slowly decaying trimer signal[1]. Hence, even the shorter lifetimes τ_6 can be determined with sufficient accuracy. In order to illustrate the large isotope effect for the ammonia trimer, we have also performed measurements on a much longer timescale for different isotopomers and determined their lifetimes in the H-transfer state. The results are shown in Figure 6.

The photoelectron signals corresponding to the $(NH_3)_m^+$ and $(ND_3)_m^+$ cluster ions after excitation by the control pulse are displayed in Figure 7. They have been

[1] In the case of a slow exponential decay the initial slope of the ion signal is unambiguously given by the solution of the Bloch equations, its half height being slightly shifted to positive time delays as compared to the maximum position of the cross correlation function [21].

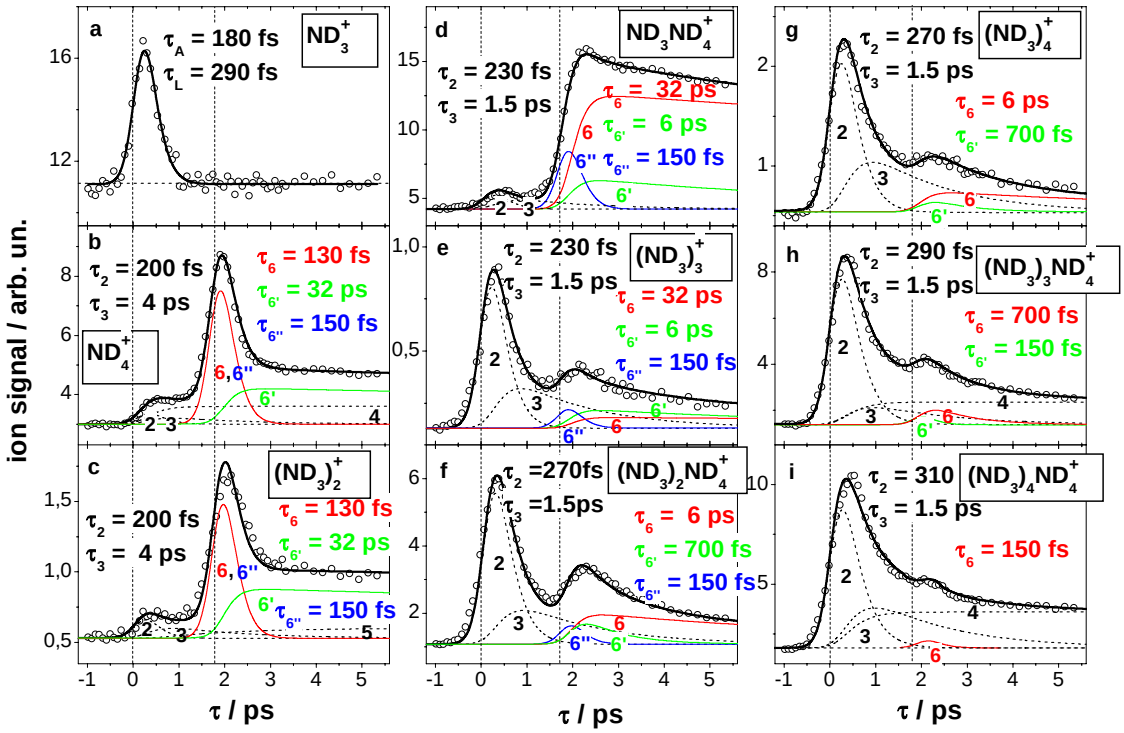

Fig. 5. Ion yield of $(ND_3)_m^+$ ($m = 1...4$; a, c, e, g, respectively) and $(ND_3)_{m-2}ND_4^+$ ($m = 2...6$; b, d, f, h, i, respectively) as function of the delay time between pump and probe pulse. The control pulse is delayed by 1.7 ps with respect to the pump. Otherwise as in Figure 4.

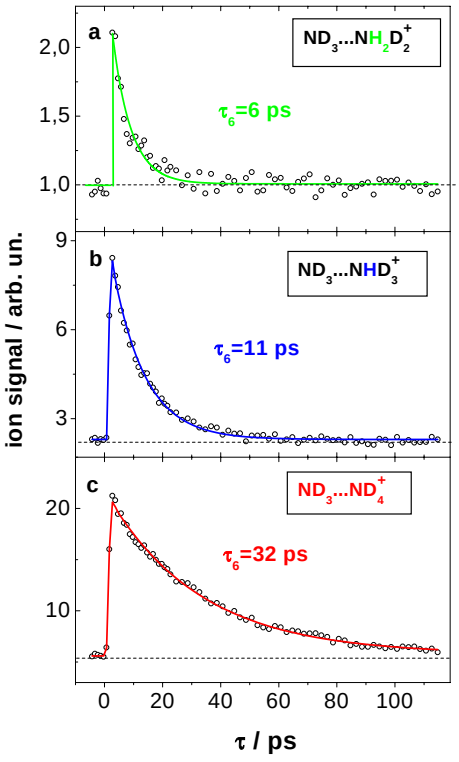

Fig. 6. Ion yield for three different isotopes ($ND_3...NH_2D_2^+$, $ND_3...NHD_3^+$ and $ND_3...ND_4^+$) as function of the delay time between pump ($\lambda_{pu} = 208$ nm) and probe pulse ($\lambda_{pr} = 416$ nm). The control pulse ($\lambda_{co}^{(1)} = 832$ nm) is delayed by 1.2 ps with respect to the pump pulse. The observed lifetimes τ_6 of the corresponding excited neutral H-transfer states of the trimers show a strong isotope dependence.

recorded at the maxima of the ion signals which have generally been observed about 100 fs after the control pulse, *i.e.* here at $\tau_{pr} = 1.3$ ps for the pump-control delay of $\tau_{co} = 1.2$ ps (*cf.* Figs. 4 and 5). In Figure 7, the background signals due to multiphoton one-color and two-color absorption are already subtracted. The experimental data represented by thick solid lines lend themselves to a fit by three Gaussian with different widths for the *ic*, the *xy* and the *z* contributions, the origin of which will be explained in the discussion section.

For the ammonia monomer NH_3 and ND_3 we have recorded PES at molecular beam expansion conditions which suppress larger clusters (only $m = 1$ and 2 observed in the mass spectra). These are shown in Figure 8 (main displays).The various lines are fitted according to well-known transitions. In contrast, the spectra shown in the inserts have been recorded for a broad cluster distribution. They clearly illustrate that the signal contributions below $E_{el} = 0.3$ eV originate from dissociative ionization of ammonia clusters in the H-transfer state. This part of the signal vanishes if the abundance of clusters is negligible or if the time-delay between the pump and the control pulse is chosen such that the H-transfer state is not populated. Below, we will attribute the low-energy parts in the PES of the ammonia complexes to the same origin as those in the monomer spectra.

3.2 Control pulse wavelength 1 200 nm

Figure 9 shows the corresponding data for a control pulse wavelength $\lambda_{co}^{(2)} = 1\,200$ nm. The raw three-color time-dependent ion signals for the $(NH_3)_m$ clusters are depicted

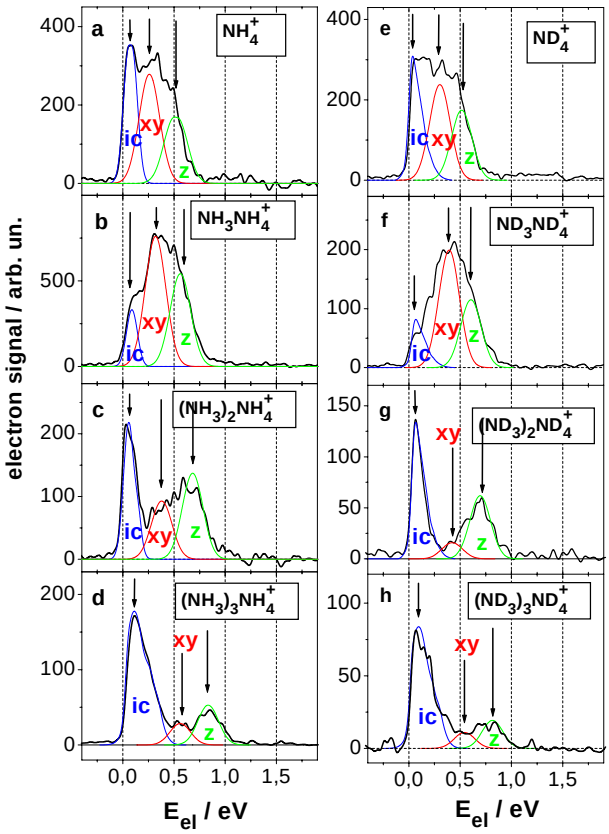

Fig. 7. *Pure* three-color (λ_{pu} = 208 nm, λ_{pr} = 416 nm, $\lambda_{co}^{(1)}$ = 832 nm) photoelectron spectra for $(NH_3)_{m-2}NH_4^+$ (a...d) and $(ND_3)_{m-2}ND_4^+$ (e...h), respectively, with $m = 2...5$. The control pulse is delayed with respect to the pump pulse by τ_{co} = 1.2 ps, the probe pulse by τ_{pr} = 1.3 ps, corresponding to the maximum of the pure three-color ion signal. The two-color background signals have been subtracted and the PES are fitted by three contributions *ic*, *xy* and *z* (see text). The arrows indicate the electron energies of the maxima of these contributions.

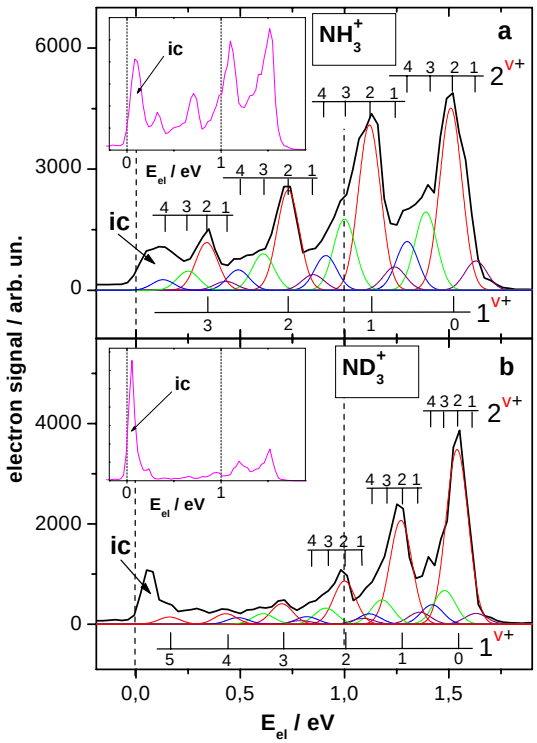

Fig. 8. Three-color (λ_{pu} = 208, λ_{pr} = 416, $\lambda_{co}^{(1)}$ = 832 nm) photoelectron spectra of (a) NH_3 and (b) ND_3, taken at delay times τ_{co} = 1.2 ps and τ_{pr} = 1.3 ps under narrow cluster distribution conditions. The peaks for electron kinetic energies above $E_{el} \geq 0.3$ eV are due to resonant one-color $2h\nu_{pu}$ absorption and assigned to $v_1\nu_1^+ + v_2\nu_2^+$ combination modes. The contribution below 0.3 eV is attributed to dissociative ionization of the ammonia clusters after absorption of $h\nu_{pu} + h\nu_{pr} + h\nu_{co}$ as well as $h\nu_{pu} + 3h\nu_{co}$. As shown in the inserts this contribution strongly increases for a broader cluster distribution obtained for a larger stagnation pressure.

in the inserts at the same time-delay as for $\lambda_{co}^{(1)}$. The dotted lines in the inserts show the two-color background which has been recorded independently without the control pulse under otherwise identical conditions. The main parts of Figure 9 show *pure* three-color signals where the two-color background has already been subtracted. Again, the various contributions to the total fit curve (bold solid line) are drawn as thin lines.

For the deuterated complexes *pure* three-color signals are shown in Figure 10. In the inserts (in contrast to Fig. 9) the *pure* three-color signals are shown on a much longer timescale. In Figure 11 the related PES for $(ND_3)_m$ clusters are presented and, similarly as for $\lambda_{co}^{(1)}$ = 832 nm, fitted approximately by a superposition of three Gaussian curves with different widths for the nonresonant *nr* and resonant *r1, r2* contributions (the undeuterated species are not shown here since they behave very similarly). The arrows pointing to the maxima of the Gaussians illustrate the shift of these signals towards higher kinetic energies with increasing cluster size.

3.3 Control pulse wavelength 1 400 nm

For $\lambda_{co}^{(3)}$ = 1 400 nm the time-dependent ion signals are shown in Figure 12 for deuterated clusters at otherwise identical cluster and laser parameters. As before, all solid lines are fits representing different contributions. Accordingly, the measured PES of $(ND_3)_m$ clusters are shown in Figure 13 together with fits derived in the same manner as for $\lambda_{co}^{(2)}$ = 1 200 nm.

Finally, in Tables 1 and 2 the decay times τ_6 of the various undeuterated and deuterated obtained in the present work are summarized for the different complex sizes m and excitation energies $h\nu_{co}$. In contrast to the dimer, which exhibits no variation of its ultrashort lifetime upon deuteration or energy change within the experimental uncertainty, for the larger clusters the decay time decreases rapidly with increasing cluster size as well as with decreasing excitation energy. This will be discussed in the following chapter.

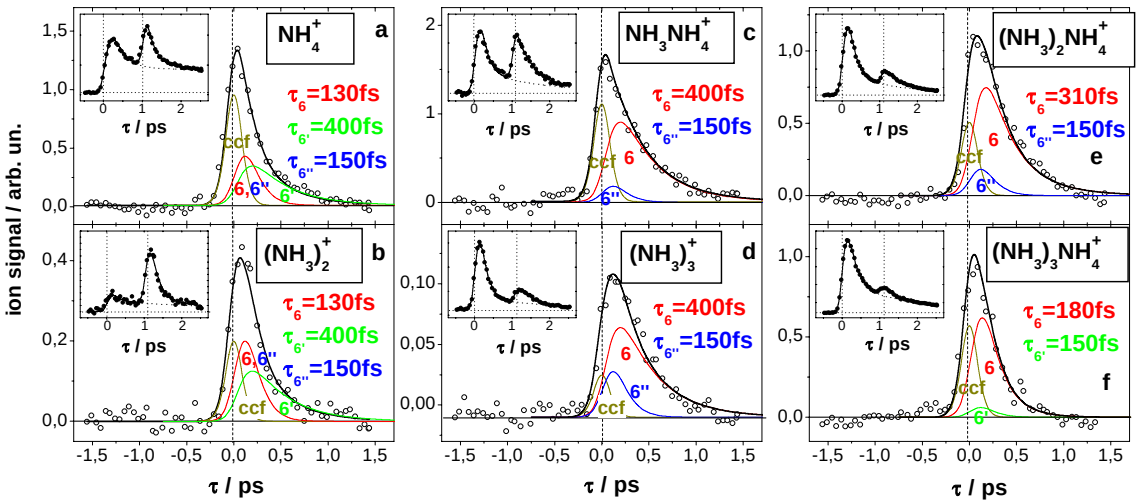

Fig. 9. *Pure* three-color ion signals of $(NH_3)_m^+$ with $m = 2$ (b) and 3 (d) and $(NH_3)_{m-2}NH_4^+$ with $m = 2$ (a), 3 (c), 4 (e) and 5 (f) as function of the delay time between control ($\lambda_{pu} = 200$ nm) and probe pulse ($\lambda_{pr} = 400$ nm). The control pulse ($\lambda_{co}^{(2)} = 1\,200$ nm) is delayed by 1.2 ps with respect to the pump. These signals are obtained by subtracting the two-color pump-probe signals from the complete ion signals displayed in the inserts. The three-color signals are formed by superposition of a nonresonant contribution (ccf), a resonant contribution (6) with the decay time τ_6 and dissociative ionization ($6'$, $6''$) with $\tau_{6'}$ and $\tau_{6''}$ as discussed in the text below. The full lines are fit curves corresponding to these different channels.

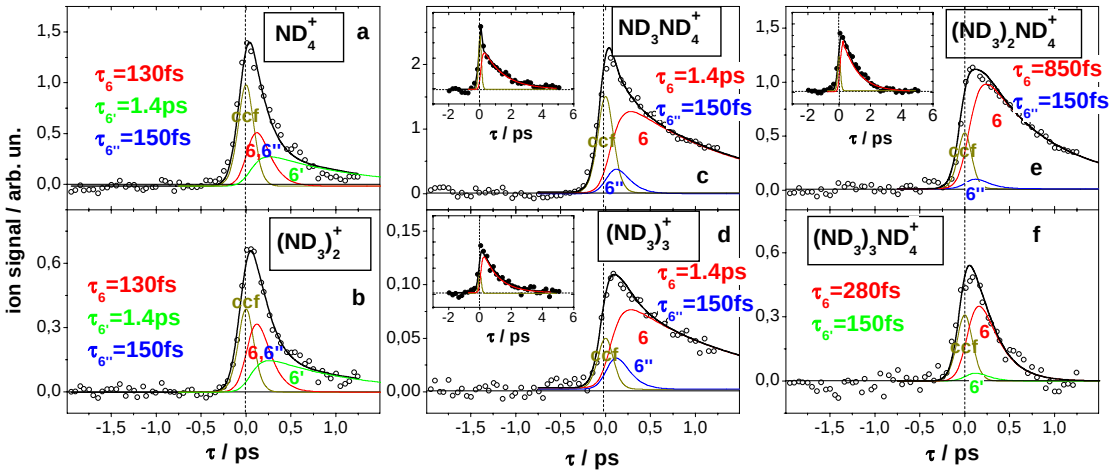

Fig. 10. *Pure* three-color ion yield of deuterated ammonia clusters *vs.* delay time τ. Here, the total ion signals are omitted, being very similar to those of Figure 9. Instead, the corresponding pure three-color on a much longer time scale are shown in the inserts. Otherwise as in Figure 9.

Table 1. Lifetimes τ_6 of the $(NH_3)_{m-2}NH_4(3p)NH_2$ states as a function of control photon energy $h\nu_{co}$.

cluster size m	τ_6/ps		
	$h\nu_{co} = 1.49$ eV	$= 1.03$ eV	$= 0.89$ eV
2	0.13 ± 0.06	0.13 ± 0.06	0.13 ± 0.06
3	2.7 ± 0.6	0.40 ± 0.06	0.32 ± 0.05
4	0.50 ± 0.15	0.31 ± 0.06	0.26 ± 0.05
5	0.250 ± 0.09	0.18 ± 0.06	0.16 ± 0.05
6	0.15 ± 0.07	0.12 ± 0.06	0.12 ± 0.06

Table 2. Lifetimes τ_6 of the $(ND_3)_{m-2}ND_4(3p)ND_2$ states as a function of the control photon energy $h\nu_{co}$.

cluster size m	τ_6/ps		
	$h\nu_{co} = 1.49$ eV	$= 1.03$ eV	$= 0.89$ eV
2	0.13 ± 0.06	0.13 ± 0.06	0.13 ± 0.06
3	32 ± 3	1.4 ± 0.3	1.0 ± 0.2
4	6 ± 2	0.8 ± 0.2	0.7 ± 0.2
5	0.7 ± 0.3	0.28 ± 0.08	0.25 ± 0.08
6	0.15 ± 0.07	0.12 ± 0.06	0.12 ± 0.06

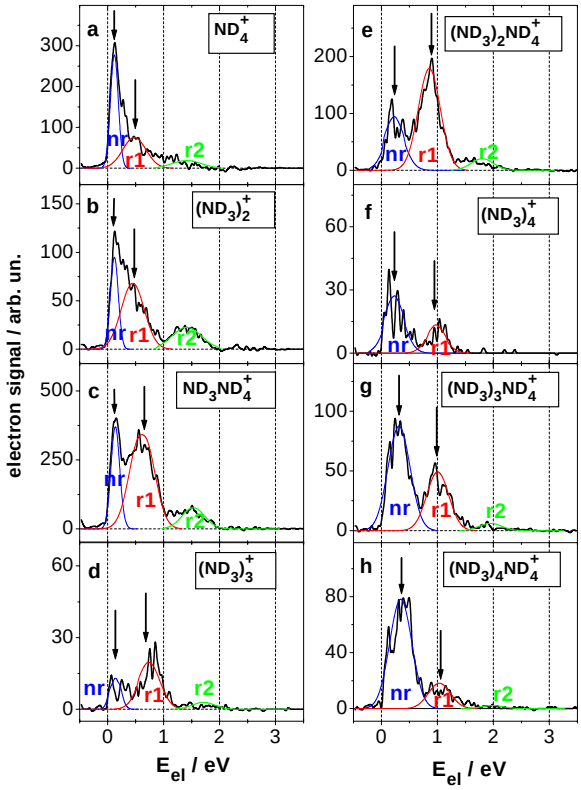

Fig. 11. *Pure* three-color (λ_{pu} = 200 nm, λ_{pr} = 400 nm, $\lambda_{co}^{(2)}$ = 1 200 nm) photoelectron spectra of $(ND_3)_m^+$ for m = 2 (b), 3 (d), 4 (e) and $(ND_3)_{m-2}ND_4^+$ for m = 2 (a), 3 (c), 4 (e), 5 (f) and 6 (g). The control pulse is delayed by τ_{co} = 1.2 ps with respect to the pump, the probe pulse by τ_{pr} = 1.3 ps. The two-color background signals have been subtracted and the PES are approximately fitted by Gaussian curves for the nonresonant (nr) and the resonant ($r1$, $r2$) contributions as explained in the text. The arrows pointing downwards illustrate the shift of the maxima towards higher energies with increasing cluster size.

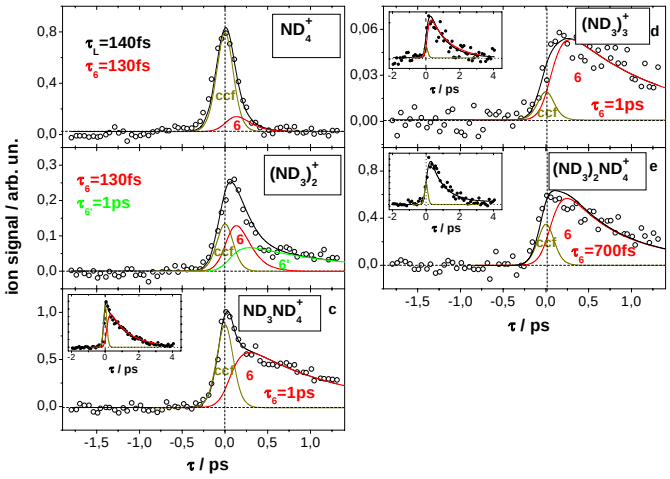

Fig. 12. *Pure* three-color ion yield of deuterated ammonia clusters *vs.* delay time τ at a control pulse wavelength $\lambda_{co}^{(3)}$ = 1 400 nm. Otherwise as Figure 10.

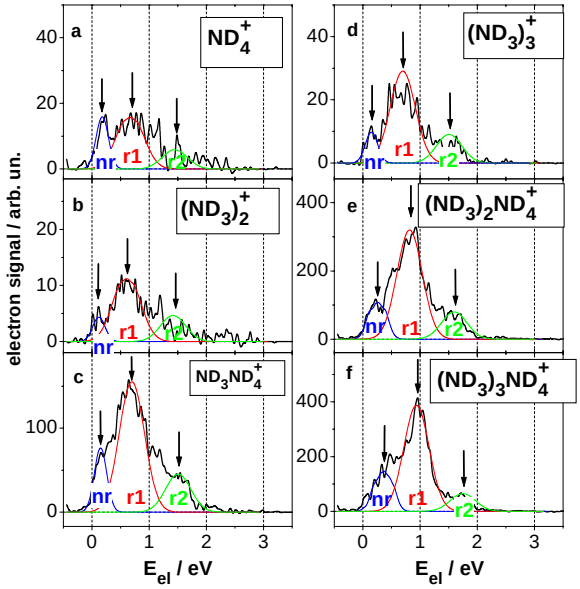

Fig. 13. *Pure* three-color photoelectron spectra of $(ND_3)_m^+$ for m = 2 (b) and 3 (d) and of $(ND_3)_{m-2}ND_4^+$ for m = 2 (a), 3 (c), 4 (e) and 5 (f) at λ_{pu} = 200 nm, λ_{pr} = 400 nm and $\lambda_{co}^{(3)}$ = 1 400 nm. Otherwise as in Figure 11.

4 Analysis and discussion

4.1 Time-dependent ion signals

The evaluation of the time-dependent ion signals (Figs. 4, 5, 9, 10 and 12) is based on the kinetic model briefly mentioned in the introduction (Fig. 2). We now discuss this model in some more detail. For a detailed justification of the model and the fitting procedures used the interested reader is referred to [21,22]. As a representative example the ammonia trimer is chosen in Figure 2 which is excited by the pump photon $h\nu_{pu}$ to its electronic $\tilde{A}$ state (2). The overall lifetime τ_2 of this state is on the order of a few 100 fs and increases slowly with cluster size [21]. The $\tilde{A}$ state (2) is depopulated *via* three different channels: dissociation into the ground state of the next smaller homogeneous cluster (configuration X), dissociation into $NH_2 + NH_3NH_4$ (4), and hydrogen migration to form the H-transfer state $NH_3NH_4(3s)...NH_2$ (3). The latter represents the main decay channel and $NH_3NH_4(3s)...NH_2$ is formed with high vibrational excitation. It decays in turn with a time constant τ_3 of a few ps by dissociation (to configuration 5 and again to X). In contrast, the population of isoenergetic levels of any electronically excited H-transfer state (6) will be negligible since such process would imply a strong change of the vibrational quantum numbers (*i.e.* a reduction of internal energy). In our kinetic model the initial excitation of state (2) is described by optical Bloch equations with a relaxation time τ_2, whereas the subsequent population of the states (3)–(5) and the following depopulation of state (3) are included by coupled rate equations [21]. The two-color pump-probe signal contributions in Figures 4 and 5 are fitted according to this model as indicated by dotted lines (corresponding

to the labels 2–5). Here, as in [22], the dimer signal is very weak, since two probe photons of $h\nu_{\rm pr} = 2.99$ eV are needed for ionization – in contrast to the signals recorded in [21] using $h\nu_{\rm pr} = 4.65$ eV as probe. In accordance with the earlier results [21] the present analysis gives lifetimes $\tau_2 = 200...310$ fs and $\tau_3 = 1.5...4$ ps (with the value of 4 ps for the dimer in the H-transfer state NH_4NH_2). During the lifetime τ_3 sufficient clusters are found in the H-transfer state (3) and can be excited electronically by the additional control photon $h\nu_{\rm co}$. Typically, the maximum population of configuration (3) is reached at about 1 to 2 ps and hence the delay between pump and control pulse has been chosen as $\tau_{\rm co} = 1.2$ ps or sometimes 1.7 ps and 2.1 ps without any significant changes of the shapes of signals as long as $\tau_{\rm co}$ was varied within this interval.

The absorption cross-section for the control photon inducing the transition

$$(NH_3)_{m-2}NH_4(3s)...NH_2 \rightarrow (NH_3)_{m-2}NH_4(3p)...NH_2$$

is large due to the large dipole moment for the $3s \rightarrow 3p$ transition of the NH_4 chromophore (having essentially Na configuration). Scanning the time-delay of the probe pulse results in time-dependent ion signals which reflect different contributions arising from the dynamics induced by the control pulse – on top of the usual two-color pump-probe signal. In Figures 4 and 5 the two-color ion signals, measured independently, are indicated as traces (2) and (3) while in Figures 9, 10 and 12 the two-color components have already been subtracted from the total ion yield in order to allow a separation of the different multiphoton contributions. These *pure* three-color signals image the additional ion intensity induced by the control pulse. They have been fitted by an analogous procedure to that described above for the two-color pump-probe evolution. The superposition of all contributions leads to the heavy solid lines which describe the data very well.

Essentially three contributions (thin solid lines) are proposed to explain the experimental observations: the lines labeled (6) in the homogeneous clusters ion signals $(NH_3)_m^+$ are attributed to the genuine contribution of the respective electronically excited $(NH_3)_{m-2}NH_4(3p)...NH_2$ for each cluster size. In contrast, the signal components labeled (6') are attributed to ionization of larger clusters by the probe laser pulse which are detected on the same mass after fragmentation by NH_3 evaporation (see introduction). This contribution (6') thus reflects the time-evolution of the corresponding parent cluster ions and not that of the cluster masses at which they are finally detected. Since the protonated ion signals $(NH_3)_{m-2}NH_4^+$ exhibit exactly the same time-dependence as the corresponding homogeneous ones, we conclude that the fragmentation process $(NH_3)_m^+ \rightarrow (NH_3)_{m-2}NH_4^+ + NH_2$ is a major formation mechanism for $(NH_3)_{m-2}NH_4^+$, which may be followed by NH_3-evaporation yielding the contributions (6'). In none of our experiments we have found a constant NH_4^+ signal at longer delay times for the pure three-color signal. This documents that all three-color induced NH_4^+ ions are due to an *AID* process (absorption, ionization, dissociation) – starting in the $NH_3NH_4(3s)...NH_2$ state – as opposed to an *ADI*–process. No NH_4 radicals are formed by dissociation of the dimer in the H-transfer configuration – neither from the excited $NH_4(3p)NH_2$ nor from the unexcited $NH_4(3s)NH_2$ state [21].

Discussing first the results for the control wavelength $\lambda_{\rm co}^{(1)} = 832$ nm (Figs. 4, 5 and 6) we note that the excited ammonia monomer isotopomers in the $\tilde{A}$ state rapidly dissociate prior to the control pulse irradiation (with lifetimes of 70 fs and 180 fs for NH_3 and ND_3, respectively [21]) and are therefore not affected by $h\nu_{\rm co}$ (*cf.* Figs. 4a and 5a). The ion signals $NH_3NH_4^+$ shown in Figure 4d (Fig. 5d for $ND_3ND_4^+$) consist of several contributions:

(i) a *true* trimer part (6) with a lifetime $\tau_6 = (2.7 \pm 0.6)$ ps [$\tau_6 = (32 \pm 3)$ ps] which originates from fragmentation of $(NH_3)_3^+$ [$(ND_3)_3^+$],
(ii) a contribution (6') with a decay time $\tau_{6'} = (500 \pm 150)$ fs [$\tau_{6'} = (6 \pm 2)$ ps] which is identical to that of the tetramer and hence is assumed to originate from dissociation of $(NH_3)_4^+$ [$(ND_3)_4^+$],
(iii) and a third contribution, labeled (6'') decaying with $\tau_{6''} = (150 \pm 70)$ fs.

We suggest that the latter contribution is caused by fragmentation of large $(NH_3)_m^+$ [$(ND_3)_m^+$] ions with $m \geq 6$, which exhibit lifetimes in this ultrashort range, whereas the lifetime of the excited pentamer is $\tau_6 = (250 \pm 90)$ fs [$\tau_6 = (700 \pm 300)$ fs]. The high amount of internal energy of the large ($m \geq 6$) cluster ions required for NH_2 loss followed by several consecutive steps of NH_3 evaporation (*cf.* introduction) can be provided by an internal conversion from the excited H-transfer state to its lowest electronic state as will be discussed in detail below. Such metastable processes do not proceed on ultrafast timescales, however, they are observed due to the residence time of the ionic complexes of several 100 ns in the ionization region of the TOF mass spectrometer.

In previous studies of the ammonia dimer (using low stagnation pressure with a narrow cluster size distribution and negligible components from higher clusters in the dimer signal) we were able to derive a lifetime of $\tau_6 = (130 \pm 60)$ fs for both isotopomers independent of the control wavelength (832 nm [28], 1 200 nm and 1 400 nm in [27]). Accordingly, in Figures 4b, 4c, 5b, and 5c this value is used as lifetime for the dimer – which coincides with those of the large ($m \geq 6$) clusters ($\tau_{6'} = (150 \pm 70)$ fs) within the experimental accuracy. We thus cannot separate these contributions in the signal of the dimer and its protonated fragment for the time being. However, from the corresponding photoelectron spectra we may glean additional information which allows us to discern the different pathways by their energetics as described below.

This simplified description of the time-dependent ion signals by three time-constants is of course only an approximative approach, subject to correspondingly high error limits for the thus determined lifetimes. Nevertheless, a consistent picture of the time-evolution and the overall trends can be extracted, which is prerequisite for

understanding the observed dynamics. In contrast to the dimer, the larger clusters are subject to pronounced isotope effects. In particular, the lifetime of the trimer increases by more than one order of magnitude upon deuteration. In Figure 6 decay curves for the protonated $ND_3ND_4^+$ (c), $ND_3NHD_3^+$ (b) and $ND_3NH_2D_2^+$ (a) are shown, reflecting the dynamics of the neutral parent homogeneous trimer complexes in the H-transfer state. The measured lifetimes τ_6 increase with the degree of deuteration from (2.7 ± 0.6) ps for $NH_3NH_4^+$ to (6 ± 2) ps (a), (11 ± 1) ps (b) and (32 ± 3) ps (c), respectively.

Turning now to excitation with the control wavelengths $\lambda_{co}^{(2)} = 1\,200$ nm and $\lambda_{co}^{(3)} = 1\,400$ nm it is again useful to include the contributions 6 and 6′ (*cf.* Figs. 9 and 10). Due to the reduced significance of cascading fragmentation from larger clusters at lower control photon energies we combine here these contributions into one constituent of the fit at $\lambda_{co}^{(2)}$ and neglect it completely at $\lambda_{co}^{(3)}$. However, an additional contribution to the signal becomes apparent as seen in Figures 9, 10 and 12, which turns out to be proportional to the cross correlation function between the control and the probe pulse, hence labeled *ccf*. As proposed in [27], we attribute this fraction of the signal to nonresonant two-photon ionization of the clusters in their H-transfer configuration $(NH_3)_{m-2}NH_4NH_2$ by the control and the probe pulse. This nonresonant *ccf* contribution was insignificant when exciting with a control wavelength $\lambda_{co}^{(1)} = 832$ nm since there the photon energy is in resonance [28] with the $3s \rightarrow 3p$ transition of the chromophore NH_4.

In principle, several rovibrational levels of the three non-degenerate $3p$ states or the $4s$ states (*cf.* [28]) may enhance the *ccf* signal. It can clearly be distinguished from the dissociative ionization of larger clusters (6′) by its different time-dependence. Even more significant, reducing the cluster size distribution to predominantly ammonia dimers [27] does not significantly affect the ratio between the resonant and the nonresonant signal components, which excludes fragmentation of larger clusters as its origin. Additional support for this interpretation is drawn from a comparison of the photoelectron spectra after excitation with $\lambda_{co}^{(1)} = 832$ nm at $\lambda_{co}^{(2)}$ and $\lambda_{co}^{(3)}$ (see below) which show that the contribution from lower ion excess energies in the *ccf* signal is much higher than the contribution (6′), and such a reduction of excess energy clearly cannot lead to increased fragmentation of the cluster ions.

In contrast to the dimer, the lifetimes τ_6 of the larger clusters in their electronically excited H-transfer states do show a strong isotope effect. In addition, they also decrease significantly when the excitation energy is reduced, *e.g.* for $(NH_3)_3$ from ∼2.7 ps [27] at $\lambda_{co}^{(1)} = 832$ nm to ∼0.4 ps at $\lambda_{co}^{(2)} = 1\,200$ nm (*cf.* Fig. 9) and ∼0.3 ps at $\lambda_{co}^{(3)} = 1\,400$ nm while for $(ND_3)_3$ we have $\tau_6 \sim 32$ ps [27], 1.4 ps (*cf.* Fig. 10) and ∼1 ps (*cf.* Fig. 12), respectively. The whole set of decay times is given in Tables 1 and 2. We conclude that completely different decay mechanisms are operative in the dimer as compared to the larger clusters.

To understand this difference we refer to our *ab initio* calculations [28] of the potential energy surfaces for the ammonia dimer and trimer for the H-transfer configuration in the relevant electronic states. The experimental data confirm the calculated transition energies by time-resolved photoelectron spectroscopy [28] and thus lend additional confidence into the *ab initio* results. As a plausible decay mechanism for the excited $NH_4(3p)...NH_2$ dimer state, the potential energy surfaces suggest a nonadiabatic transition through a surface-crossing (more strictly speaking: a conical intersection) with the repulsive $NH_4(3s)...NH_2(2p_z)$ state. In contrast to the bound $NH_4(3s)...NH_2$ state with the NH_2 constituent being in its ground electronic state and the unpaired electron oriented perpendicularly to the NH_2 plane, $NH_2(2p_z)$ denotes the first excited state of the NH_2 radical, its unpaired $2p$ electron being oriented along the NH_2 symmetry axis (z-direction). We note that the three-fold degeneracy of the $NH_4(3p)$ state is removed due to the presence of NH_2 and a series of crossings is energetically accessible at sufficiently large H–N–H angles, *i.e.* if the corresponding bending mode is excited during the H-transfer process. Such a mechanism can readily explain the very short lifetime (∼0.13 ps) of $NH_4(3p)NH_2$. It also gives a plausible argument for the negligible influence of deuteration and changes in the excitation energy.

In contrast, for ammonia trimers our calculations [28] show that the coupling between the initially excited potential energy surface $NH_4(3p)NH_2$ H-transfer state to the next higher repulsive $NH_4(3s)NH_2(2p_z)$ state is not accessible at reasonable H–N–H bending angles. Although in principle, such crossing might be reached at huge H–N–H bending angles of NH_2 *via* tunneling of far wings of the wave-function, the experimental findings of this work contradict such an injection: (apart from the dimer) the observed lifetime of the electronically excited H-transfer state decreases rapidly (a) with increasing cluster size and (b) with reduced excitation energies. For tunneling just the opposite would be expected. Thus we propose an internal conversion mechanism for explaining the decay of the excited $(NH_3)_{m-2}NH_4(3p)NH_2$ back to the lowest $(NH_3)_{m-2}NH_4(3s)NH_2$ H-transfer state which is then followed by dissociation of the ammonia clusters. This suggestion is compatible to the observations and will be further discussed below. It should be noted that the same mechanism, in principle, could also occur in the ammonia dimer. However, due to the comparatively low density of states it would be effective on a much longer timescale which cannot compete with the ultrafast channel *via* curve crossing described above.

4.2 Time-resolved photoelectron spectra

The corresponding photoelectron spectra (PES) can elucidate the energetics underlying the ammonia cluster dynamics and justify the preceding assignments of the ion signal contributions. The discussion is based on the energy schemes depicted in Figures 14 and 15 where the energy

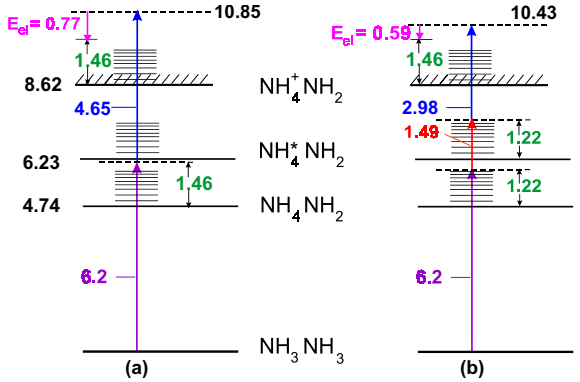

Fig. 14. Energy scheme for the H-transfer configuration of the ammonia dimer as relevant to the interpretation of the observed PES for $\lambda_{co}^{(1)} = 832$ nm, *i.e.* $h\nu_{co}^{(1)} = 1.49$ eV. All numbers given in the diagram refer to energies in eV. Photons and electrons are represented by arrows pointing upwards and downwards, respectively, the lengths of which reflects the corresponding energies. For reference the case without irradiation of a control photon but with accordingly higher probe photon energy is illustrated in (a). The amount of vibrational energy deposited in the H-transfer state has been revealed by PES, *cf.* [27]. The three color pump-control-probe scheme (b) is based on the previously determined transition energy to the first excited electronic state NH_4^* NH_2, *i.e.* the $NH_4(3p)$...NH_2 state [27].

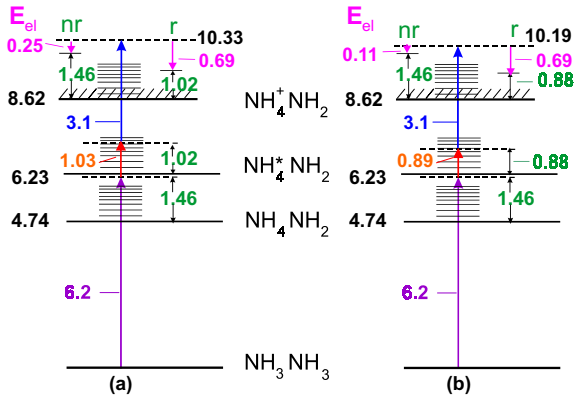

Fig. 15. Energy scheme for the three color excitation scheme of the H-transfer state of the ammonia dimer. Control photon energies of $h\nu_{co}^{(2)} = 1.03$ eV (a) and $h\nu_3^{(3)} = 0.89$ eV (b) are illustrated. We distinguish between the nonresonant (nr) and resonant (r) absorption of the control and probe photons. Otherwise as in Figure 14.

levels of the lowest ($3s$) and first excited ($3p$) neutral H-transfer state and that of the ionic proton transfer state as calculated in our previous studies [25,28] are represented for the ammonia dimer. The different photon energies as well as the related internal ionic and photoelectron kinetic energies are indicated as derived from Franck-Condon considerations and energy conservation.

In [25] the ammonia dimer was excited with pump photons $h\nu_{pu} = 6.2$ eV (200 nm), leading to a vibrational excitation of 1.46 eV in the $3s$ H-transfer state after the initial rearrangement process being completed as schematically indicated in Figure 14a. The thus induced dynamics and the underlying energetics was probed by $h\nu_{pr} = 4.65$ eV (267 nm) photons. Referring to our calculations in [25], the structures of the H-transfer state and the proton transfer configuration in the ionic ground state do not differ essentially from each other, and accordingly the corresponding potential energy surfaces have very similar shapes and minimum energy positions. As a consequence, we expect and in fact observe a *propensity for the vibrational energy to remain unchanged*, *i.e.* the internal energy of 1.46 eV in the H-transfer state will essentially remain unchanged in the ion state. The kinetic energy of the corresponding photoelectrons is derived from the energy balance

$$E_{kin}^{el} = h\nu_{pu} + h\nu_{pr} - IP - E_{vib},$$

with E_{vib} being the internal energy and $IP = 8.62$ eV the adiabatic ionization potential with respect to the ground state of $(NH_3)_2$. Thus, these considerations predict the photoelectron spectrum to peak at 0.77 eV and indeed, the maximum of the observed distribution was found at about 0.7 eV [25].

With these previous results in mind, we now focus on Figure 14b. Exciting with a pump photon of $h\nu_{pu} = 5.96$ eV ($\lambda_{pu} = 208$ nm) the vibrational energy in the $NH_4(3s)$...NH_2 configuration amounts to 1.22 eV. For the subsequent electronic excitation by the control photon of $h\nu_{co}^{(1)} = 1.49$ eV ($\lambda_{co}^{(1)} = 832$ nm) as well as for the ionization by a probe photon of 2.98 eV (416 nm) the above discussed propensity rule will also apply and we expect the vibrational energy to be approximately conserved ($\Delta v = 0$). Hence, the experimental PES should peak at 0.59 eV. Figure 7 shows the three-color PES of (a) NH_4^+, (b) $NH_3NH_4^+$ (c) $(NH_3)_2NH_4^+$ and (d) $(NH_3)_3NH_4^+$, while Figures 7e–7h display their deuterated counterparts, respectively, with the one- and two-color background signals already subtracted. These spectra have been obtained with the control pulse delayed by 1.2 ps with respect to the pump pulse. The probe pulse (photon energy $h\nu_{pr} = 2.98$ eV, $\lambda_{pr} = 416$ nm) had a time-delay $\tau_{pr} = 1.3$ ps corresponding to the maximum of the dimer three-color ion signals (*cf.* Figs. 4c and 5c). The characteristic threefold structure which has already been observed in the two-color case [28] is attributed to three processes labeled *ic*, *xy* and *z*, which are again approximated by three Gaussian fit curves. As in reference [28] we attribute the signals *xy* and *z* to the non-degenerate $3p_x$, $3p_y$ and $3p_z$ states of the chromophore NH_4 in the clusters which is excited by the control photon $h\nu_{co}^{(1)}$ and subsequently ionized by the probe photon, confirming the $3s \rightarrow 3p$ transition energy of 1.5 eV for the dimer. As function of cluster size we observe a shift of these signals towards higher photoelectron kinetic energies (as indicated by the arrows pointing on the maxima of the Gaussians). This is to be expected due to decreasing ionization potentials of the larger clusters and essentially constant vibrational energies.

The third contribution *ic* is of different origin, as a comparison for different cluster sizes clearly reveals: it is just barely discernible (at very low electron energies) for the dimer and trimer (Figs. 7a, 7b, 7e and 7f) but

becomes very distinctive for the fragments of the tetramer (Figs. 7c and 7g) and pentamer (Figs. 7d and 7h). Nonresonant multi-photon ionization can be ruled out as source of the *ic* contribution: in such a case vibrational energy in the $NH_4(3s)...NH_2$ H-transfer state (1.22 eV as indicated in Fig. 14b) will essentially be transferred into the ionic ground state due to the propensity rule. The corresponding photoelectrons would appear in the PES at kinetic energies above 0.5 eV, in particular for larger clusters with their lower adiabatic ionization potentials. In contrast, the sharp *ic* peak in Figures 7c and 7g at very low energies corresponds to an internal energy of the $(NH_3)_2NH_4^+$ ions which is at least 0.7 eV higher than the 1.22 eV in the initial configuration of the H-transfer state. At such high vibrational energies fragmentation in the cluster ions is very likely to occur and leads to stabilization of the cluster ions. Thus, a considerable part of the low-energy photoelectrons detected at a given mass originate from larger ammonia complexes with lower adiabatic ionization potential. Due to the propensity rule ($\Delta v \sim 0$) for ionization such vibrational energies of more than 2 eV in the cluster ions originate from about the same vibrational energy in the neutral precursor – an energy which is substantially higher than that expected in the $(NH_3)_{m-2}NH_4(3p)NH_2$ H-transfer state originally excited by the control photon. Thus, we attribute the *ic* process to internal conversion from this state back to the lowest $(NH_3)_{m-2}NH_4(3s)NH_2$ H-transfer state which is then ionized by the probe photon. In a final step the highly vibrationally excited ammonia cluster ions dissociate. This interpretation of the *ic* process is further corroborated by the dependence of the observed excited state lifetimes on excitation energy, clusters size and deuteration. Further details will be discussed in the following section.

Additional support for this assessment originates from the PES of the ammonia monomers NH_3 and ND_3 shown in Figures 8a and 8b, respectively. In these spectra, recorded under expansion conditions for a narrow cluster size distribution [28], all the peaks at kinetic electron energies above 0.3 eV result exclusively from resonant one-color two pump photon absorption by the ammonia monomers which has been confirmed by separate one-color experiments. In [28] these features have been assigned to progressions in the well-known ν_2^+ out-of-plane bending mode as well as to $\nu_1^+ + v_2\nu_2^+$ vibrational combination transitions and fitted by Gaussians. The signal below 0.3 eV does not appear in one-photon ionization with $h\nu_1$ unless control and probe pulses with a sufficiently large time-delay (*e.g.* 1.2 ps) are also applied. Note that at this delay-time all excited $\tilde{A}$ state population of the excited ammonia monomer has long been lost due to ultrafast dissociation within about 40 fs for NH_3 and 180 fs for ND_3 [21]. Thus, the origin of these *three-color* photoelectrons is related to the H-transfer dynamics of the ammonia clusters which occurs on a picosecond time scale, and not to ionization of the monomers. This conclusion is further corroborated by a comparison of the PES in Figures 8a and 8b with those in the respective inserts. The latter have been obtained for the broad cluster distributions of the present work and show a drastic increase of the contribution *ic*. Obviously we see here also a fingerprint of the mechanism responsible for the *ic* signal in the spectra of larger cluster ions, *i.e.* dissociation after ionization of highly vibrationally excited clusters populated by internal conversion. Due to the high internal energy in the ion several cluster sizes may contribute to the monomer (and small cluster) ion signal *via* successive NH_3 evaporation (*cf.* Sect. 1), accumulating in a strong *ic* peak.

We now turn to the PES measured at $\lambda_{co}^{(2)} = 1\,200$ nm ($h\nu_{co}^{(2)} = 1.03$ eV, *cf.* Fig. 11) and $\lambda_{co}^{(3)} = 1\,400$ nm ($h\nu_{co}^{(3)} = 0.89$ eV, *cf.* Fig. 13). The energy scheme for the ammonia dimer shown in Figure 15 is similar to that of Figure 14. Due to the different energetics we will have to attribute some of the contributions observed in the PES to different mechanisms. As shown in [27] a control photon energy of $h\nu_{co}^{(2)} = 1.03$ eV or $h\nu_{co}^{(3)} = 0.89$ eV leads to a reduction of the vibrational energy in the electronically excited $NH_4(3p)...NH_2$ H-transfer state with respect to the electronically lowest $NH_4(3s)...NH_2$ H-transfer state: despite the smaller Franck-Condon factors for these transitions the $3s \rightarrow 3p$ transition probability is still sufficiently high because of the large electronic transition dipole moment of the NH_4 chromophore. We now have to distinguish between

1. resonant absorption *r* of the control photon (1.03 eV or 0.89 eV) and subsequent ionization by the probe photon ($h\nu_{pr}^{(2)} = 3.1$ eV) and
2. nonresonant *nr* 2-photon ionization by control and probe photon.

In the latter case the excited H-transfer state is not populated and the vibrational energy of 1.46 eV in the H-transfer state is transferred to the ion state according to the propensity rule. The resulting electron energies are ∼0.25 eV or ∼0.11 eV for $h\nu_{co}^{(2)} = 1.03$ eV or $h\nu_{co}^{(3)} = 0.89$ eV, respectively. In contrast, the resonant *r* population of the excited H-transfer state leads to a reduction of the vibrational energy to ∼1.02 eV or ∼0.88 eV for $h\nu_{co}^{(2)} = 1.03$ eV or $h\nu_{co}^{(2)} = 0.89$ eV, respectively. Hence, after ionization by the probe photon we expect the kinetic electron energies of the ejected electrons to peak at ∼0.69 eV in both cases as evident from Figure 15. A comparison of the *nr* and *r1* peaks in the experimentally observed PES (Figs. 11a, 11b, 13a and 13b) confirms these assessments – considering the relatively broad Franck-Condon region for the resonant electron spectra and the uncertainty of the theoretical energy determination of the excited state energy (±0.1 eV). The ratio of the nonresonant and resonant signal contributions to the PES agrees quite well with that derived from the respective contributions of the fit to the time-dependent ion signals (*cf.* the preceding section).

In addition to the structures labeled *r1*, the PES of Figures 11 and 13 exhibit a further resonant structure *r2* of about the same spectral width. The energy difference between the two resonant structures amounts almost exactly to the energy of the control photons $h\nu_{co}^{(2)} = 1.03$ eV

and $h\nu_{\rm co}^{(3)} = 0.89$ eV, respectively. We thus attribute this contributions *r2* to an absorption of two control photons. Since the $3s \rightarrow 3p$ transition is saturated under our experimental conditions (as confirmed by measuring its intensity dependence), such a second absorption is expected. It leads into a dense manifold of higher Rydberg states with similar nuclear geometries and thus correspondingly unchanged vibrational energies. Since this vibrational energy is transferred to the ionic ground state, according to the propensity rule the excess energy is released to the ejected photoelectron giving rise to the *r2* peaks.

We turn now to the PES for the larger ammonia cluster shown in Figures 11c–11h and 13c–13f. A comparison with the dimer spectra (Figs. 11a, 11b, 13a and 13b) shows again a significant and increasing shift of the resonant peaks to larger electron energies as already discussed for $h\nu_3^{(1)} = 1.49$ eV. This shift reflects the cluster size-dependent reduction of the adiabatic ionization potential of the chromophore NH_4 due to the solvent NH_3 molecules of up to about 0.6 eV for 4 solvent molecules (compare Figs. 11a and 11h). The perturbation of NH_4 by NH_2 in the H-transfer configuration is comparable to that of a NH_3 molecule. The solvent cage also causes the observed differences in the dynamics of the various cluster sizes which will be discussed in the following.

In addition to these processes we also have to consider the contribution due to fragmentation of larger clusters after internal conversion *ic* as discussed for the higher excitation energy $h\nu_{\rm co}^{(1)}$. We believe that such fragmentation is less important for the excitation energies $h\nu_{\rm co}^{(2,3)}$ due to the reduced excess vibrational energy. In the PES such a contribution would correspond to very low electron energies and obviously cannot be distinguished from the *nr*-component.

4.3 Decay mechanism of $(NH_3)_{m-2}NH_4(3p)NH_2$

In the preceding subsections we have proposed an internal conversion process from the excited $(NH_3)_{m-2}NH_4(3p)NH_2$ state back to the $(NH_3)_{m-2}NH_4(3s)NH_2$ state (followed by rapid dissociation) to provide an efficient decay mechanism for the electronically excited H-transfer configuration. The argument was on the one hand based on the observation of low photoelectron energy peaks in the PES related to very high vibrational energies of the corresponding photoions (by virtue of the propensity rule, corresponding to about the same internal energies in the neutral states prior to ionization). On the other hand, the dependence of the lifetimes of the $(NH_3)_{m-2}NH_4(3p)$ NH_2 states on the cluster size and excitation energy (summarized in Tab. 1) as well as the large isotope effect (*cf.* Tab. 2) give additional support to an *ic*-mechanism. In the following, we will outline in some more detail a simple theoretical model illustrating that the observed trends are indeed compatible with the proposed mechanisms.

Figure 16 schematically indicates the non-adiabatic coupling between an (excited) vibrational level v_I in the electronic state I with a set of levels v_{II} in the electronic state II due to non Born-Oppenheimer terms.

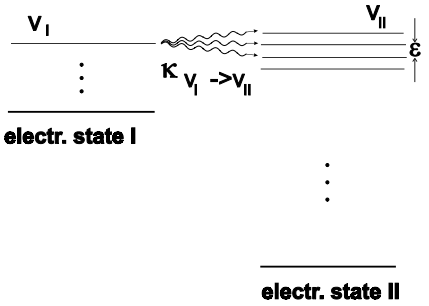

Fig. 16. Model for the non-adiabatic coupling between two electronic states I and II. v_I is the vibrational quantum number of state I, v_{II} of state II and $\kappa_{v_I \rightarrow v_{II}}$ the non-adiabatic coupling matrix element. The quantity ε denotes the level spacing in the quasi-continuum of the electronic state II. Energy conservation is fulfilled by participation of low-energy modes.

The coupling is characterized by the matrix element $\kappa_{v_I \rightarrow v_{II}}$ and the energetic separation of the v_{II} vibrational levels in the quasi-continuum of electronic state II is characterized by ε. For simplicity and because we are interested in the case of $\varepsilon \rightarrow 0$ the restriction to a constant (average) value of ε is sufficient and we further assume that $\kappa_{v_I \rightarrow v_{II}}$ does not depend on v_{II}. If at time $t = 0$ the v_I state is populated (100%), the population varies with time as $\mathrm{e}^{-\Gamma_{ic} t}$, where according to Fermi's Golden Rule

$$\Gamma_{ic} = \frac{2\pi}{\hbar} \lim_{\varepsilon \rightarrow 0} \frac{\left|\kappa_{v_I \rightarrow v_{II}}\right|^2}{\varepsilon}$$

(assuming $\left|\kappa_{v_I \rightarrow v_{II}}\right|^2 \gg |\varepsilon|^2$).

The coupling matrix element between the vibronic levels v_I and v_{II} is given by (*cf.* [32] and references therein):

$$\widehat{\kappa} = -\sum_i \frac{\hbar^2}{m_i} K_{I \longleftrightarrow II}^{(i)} \widehat{\frac{\partial}{\partial R_i}}, \text{ where}$$

$$K_{I \longleftrightarrow II}^{(i)} = \int \varphi_I^* \left(R_i, r_{\rm el}\right) \frac{\partial}{\partial R_i} \varphi_{II} \left(R_i, r_{\rm el}\right) \mathrm{d}r_{\rm el}$$

with R_i being the nuclear coordinate connected to the motion of the mass m_i, $r_{\rm el}$ the electronic coordinates, φ_I and φ_{II} the electronic wave-function of states I and II, respectively, (φ_I and φ_{II} depend on R_i parametrically) and $K_{I \longleftrightarrow II}^{(i)}$ the electronic part of $\kappa_{v_I \rightarrow v_{II}}$.

The non-adiabatic coupling matrix element between the nearly isoenergetic vibronic states can be further expressed by

$$\kappa_{v_I \rightarrow v_{II}} = \int \ldots \int \Psi_{I,v_I}^{\rm vib*} \left(R_1, \ldots, R_i, \ldots R_s\right) \times \left[-\sum_i \frac{\hbar^2}{m_i} K_{I \longleftrightarrow II}^{(i)} \frac{\partial}{\partial R_i}\right] \times \Psi_{II,v_{II}}^{vib} \left(R_1, \ldots, R_i, \ldots R_s\right) \mathrm{d}R_1 \ldots R_i \ldots R_s$$

where $\Psi_{I,v_I}^{\rm vib}$ ($\Psi_{II,v_{II}}^{\rm vib}$) is the vibrational wave-function of the electronic states $I(II)$. It is reasonable to separate

the translational and rotational degrees of freedom and to consider only the s vibrational degrees of freedom.

After introduction of normal coordinates ξ and approximating the vibrational system by s uncoupled harmonic oscillators, for the so-called promoting mode p with its normal coordinate ξ_p the integral

$$\int \Psi^{\mathrm{vib}*}_{I,v'_p}(\xi_p)\,\frac{\partial}{\partial\xi_p}\Psi^{\mathrm{vib}}_{II,v''_p}(\xi_p)\,\mathrm{d}\xi_p$$

is negligibly small except $v'_p = v''_p \pm 1$. For the remaining $s-1$ vibrational coordinates we obtain overlap integrals

$$\int \Psi^{\mathrm{vib}*}_{I,\nu'}(\xi)\,\Psi^{\mathrm{vib}}_{II,\nu''}(\xi)\,\mathrm{d}\xi$$

leading to $v''_p - v'_p = 0$ if there are no changes of the equilibrium geometry and vibrational frequencies between both electronic states.

When applying these relations to the ammonia cluster system by identifying the $(NH_3)_{m-2}NH_4(3s)NH_2$ and $(NH_3)_{m-2}NH_4(3p)NH_2$ states with the electronic states II and I, respectively, we recall that according to our *ab initio* calculations [28] the *intramolecular* vibrational frequencies and equilibrium geometries are nearly the same for both states. Significant geometry changes are expected only for the *intermolecular* degrees of freedom. However, their vibrational frequencies are low ($\hbar\omega_{\mathrm{vib}} \lesssim 0.05$ eV) compared to the $3s \longleftrightarrow 3p$ energy gap which is on the order of 1 eV. On the other hand, the energy difference between the electronic states I and II has to be converted into vibrational energy of state II. The highest (intramolecular) vibrational frequency is that of the N−H stretching mode (∼0.4 eV). Assuming that this mode is the promoting mode ($\Delta v = \pm 1$) and taking into account the $3s \longleftrightarrow 3p$ energy gap of about 1 eV, an additional vibrational excitation of the $3s$ state of about 1 eV − 0.4 eV = 0.6 eV is required. Because of the poor values of the overlap integrals (see above) the resultant rate should be relatively small and hence, it would thus be difficult to understand lifetimes of less than 10 ps.

However, if we consider the anharmonicity of the promoting mode we may have $\left|v''_p - v'_p\right| > 1$ with the restriction that the corresponding non-adiabatic coupling matrix element should be reduced for larger $\left|v''_p - v'_p\right|$. Thus, the resulting rate Γ_{ic} will decrease with increasing energy separation between the vibrational levels of the $3s$ and $3p$ electronic states. The remaining energy mismatch between the interacting vibronic levels is compensated by the energy exchange of the intermolecular vibrations. The relevant promoting modes should be the N−H stretching modes because they have the highest vibrational frequencies in the ammonia cluster system. This plausible assumption is supported by the experimental finding of a large isotope effect for the lifetime of medium-sized clusters. Obviously, $v''_p - v'_p$ is larger in the deuterated case due to the lower N−D stretching frequency, hence the higher lifetime of the excited deuterated clusters observed experimentally.

This also explains the remarkable reduction of the $(NH_3)_{m-2}NH_4(3p)NH_2$ lifetime for $m > 2$ (the dimer being a special case as discussed above): with increasing cluster size the $3s \longleftrightarrow 3p$ energy gap decreases (in analogy to the adiabatic ionization potentials) [28] and hence, internal conversion from the $3p$ state back to the $3s$ state becomes more efficient.

One may wonder whether such an internal conversion can proceed with time constants of less than 200 fs observed for the large clusters. Indeed, an additional process might precede the internal conversion. For larger clusters we expect the excited electron, *i.e.* the charge distribution of the NH_4 valence electron is spatially separated from the NH_4^+ ion core and the electron may be distributed over the cluster. In that case we expect a time dependence of the excited $(NH_3)_{m-2}NH_4(3p)NH_2$ state to originate from two processes:

1. initial dynamics due to reorientation of the *solvent* ammonia molecules after excitation of the p state (because the charge distribution of the p electron differs from that in the s state),
2. non-adiabatic $p \rightarrow s$ interaction.

As an ultrafast restructuring of the ammonia solvent cage goes along with a change of the cluster geometry, the Franck-Condon factors for ionization should also vary accordingly, resulting in a broadening of the PES of the very large clusters as well as in the low-energy peaks *ic* in the spectra of the small ones (corresponding to high ionic vibrational energies, which are necessary for several consecutive fragmentation steps).

Finally, we discuss the experimentally observed decrease of the $(NH_3)_{m-2}NH_4(3p)NH_2$ lifetimes τ_6 with decreasing excitation energy $h\nu_{\mathrm{co}}$ (*cf.* Tabs. 1 and 2). As before, when explaining the decrease of τ_6 with increasing cluster size (at a fixed excitation energy), we hold the energy gap between the involved electronic states responsible. However, with reference to the observed PES, it appears unlikely that electronic states higher than the $3p$ state are involved in such a process: the higher electronic energy would imply lower vibrational and thus, a correspondingly larger photoelectron energy. This is not observed in the PES. Therefore, we propose that a larger *effective* energy gap between the $3s$ and the $3p$ states has to be taken into account, rather than different electronic states. In order to illustrate this point we show for the H-transfer state in the trimer in Figure 17 (adopted from our *ab initio* calculations [28]) a cut through the $3s$ and $3p$ potential energy surfaces along the N−N coordinate (distance $r_{\mathrm{N-N}}$ between the nitrogen atoms of NH_4 and NH_3). Due to the perturbation by NH_2 the three-fold degeneracy of the $3p$ state in the chromophore NH_4 is removed. The $3p_z$ orbital is oriented along the other N−N direction (that between the NH_4 and the NH_2 whereas the $3p_x$ and $3p_y$ orbitals are both perpendicular to this line, the $3p_x$ lying in the NH_2 plane, the $3p_y$ perpendicularly to it. As can be seen in Figure 17 the $3s \longleftrightarrow 3p$ transition energy $\Delta E^{(0)}$ at the equilibrium geometry is considerably smaller than the energy difference between the $3s$ and the $3p$ states for large values of $r_{\mathrm{N-N}}$ because the $3p$ potential wells are much steeper, *i.e.* the $3p$ states are characterized by

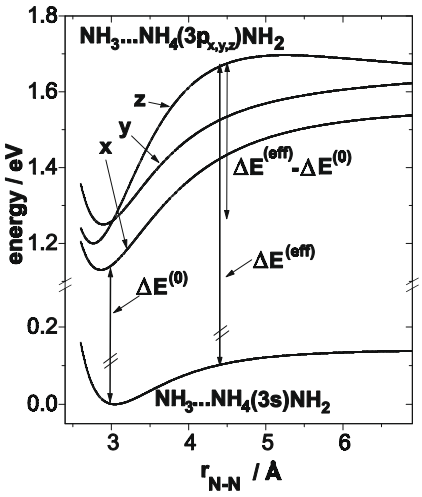

Fig. 17. *Ab initio* calculated potential curves (adopted from Ref. [28]) of $NH_3NH_4NH_2$ in the ground state ($3s$) and in the first three excited electronic states ($3p_x, 3p_y, 3p_z$) as a function of the N–N distance r_{N-N} between NH_3 and NH_4. $\Delta E^{(0)}$ denotes the minimum $3s \longleftrightarrow 3p$ transition energy at the equilibrium geometry, $\Delta E^{(\mathrm{eff})}$ the effective gap at higher excitation energies, the difference $\Delta E^{(\mathrm{eff})} - \Delta E^{(0)}$ is proposed to cause the observed longer lifetime at higher control photon energies $h\nu_{\mathrm{co}}$.

a larger binding energy than the $3s$ state. Between these two limits the effective vertical transition energy $\Delta E^{(\mathrm{eff})}$ depends on the excited sublevel (x, y, z) of the $3p$ states and also on the distance r_{N-N}, *i.e.* on the excitation of intermolecular modes.

Due to Franck-Condon restrictions, the ammonia cluster in their H-transfer state will be excited by low-energy control photons preferentially to the $3p_x$ state near the equilibrium geometry, *i.e.* the corresponding electronic transition energy should be near to the minimum value $\Delta E^{(0)}$. In contrast, for higher control photon energies it can be assumed that mainly the $3p_z$ state will be populated at larger r_{N-N} values. Two effects may lead to such a larger mean r_{N-N} distance.

i. The initial geometrical rearrangement process populates a *hot* H-transfer configuration with inter- and intramolecular modes excited. Due to the Franck-Condon rule and the greater steepness of the $3p$ potential well compared to that of the $3s$ state higher excitation energies will favor vertical transitions from higher intermolecular vibrational levels. The latter are connected with a maximum probability at larger r_{N-N} values (turning points of a *classical* harmonic oscillator).
ii. For the intermolecular vibrational levels of the excited states the internal conversion back to the $3s$ state will be preferred at their points of maximum probability density, *i.e.* for higher levels at longer r_{N-N} distances and accordingly at larger effective energy gaps.

Thus, the difference $\Delta E^{(\mathrm{eff})} - \Delta E^{(0)}$, describing an effective energy gap which increases with the excitation energy, can cause the prolongation of the $(NH_3)_{m-2}NH_4(3p)$ ...NH_2 state lifetimes at higher control photon energies $h\nu_{\mathrm{co}}$.

However, since we do not know the intrinsic vibrational distributions in the $(NH_3)_{m-2}NH_4(3s)$...NH_2 state (after the H-transfer and before control pulse irradiation), this explanation remains tentative and qualitative. A quantitative comparison, *e.g.* using the predictions of the energy gap law (*cf. e.g.* [34,35]), is impossible at present since the initial configuration (geometries, vibrational excitation) of the hot ammonia complexes in their H-atom transfer state is essentially unknown.

It appears very interesting to compare the H-transfer states in ammonia cluster to solvated metal atoms in a finite environment – another type of cluster system, which albeit different, shows a number of intriguing parallels to those presently studied. We note that *e.g.* in $Na(NH_3)_m$ clusters for which dynamic studies have recently been reported (*cf.* [36,37]) the sodium atom acts as chromophore in the NH_3 cage. Na is isoelectronic to NH_4 and in both cases an unpaired $3s$ electron is excited to a $3p$ orbital which is perturbed by the ammonia solvent molecules. By pump-probe techniques, Schulz *et al.* [36,37] have determined the corresponding lifetimes of the $Na(NH_3)_m$ complexes, revealing time constants of $\tau = 1.1$ ns for $NaNH_3$, $\tau = 33$ ps for $Na(NH_3)_2$ and $\tau = 1.1$ ps for $Na(NH_3)_3$. The lifetimes of the larger clusters finally decrease to about 120 fs. In these experiments too, a huge isotope effect of has been observed ($\tau_{\mathrm{D}}/\tau_{\mathrm{H}} = 75$ for $Na(NH_3)_2$) which reduces to about 1.5 for large $Na(NH_3)_m$ clusters ($m \geqslant 9$). There, internal conversion was also considered as one possible mechanism for the observed decay. Independent of whether this actually holds in either of these systems, the striking analogies in the molecular and the metal atom-molecule clusters strongly suggest that the same mechanism might be responsible for the observed dynamics.

5 Conclusion

In this work we have studied the dynamics and energetics of ammonia clusters and their deuterated isotopomers in their H-transfer configuration. About 1 to 2 ps after excitation to their electronic $\tilde{A}$ state by 208 nm femtosecond laser pump pulses, *i.e.*, when the transfer from the initially populated $\tilde{A}$ state to the H-transfer configuration is completed, the clusters are electronically excited by IR control pulses of variable wavelength. For detection the clusters are subsequently ionized by a third probe pulse of 416 nm.

Analyzing the time-dependent ion signals at $\lambda_{\mathrm{co}}^{(1)} = 832$ nm ($h\nu_{\mathrm{co}}^{(1)} = 1.49$ eV), for the trimer in its $(NH_3)NH_4(3p)NH_2$ state a lifetime of about (2.7 ± 0.6) ps is obtained which changes drastically to (32 ± 3) ps upon deuteration. The lifetime decreases rapidly with increasing cluster size down to (150 ± 70) fs already for the hexamer. Decreasing the excitation energy to $h\nu_{\mathrm{co}}^{(2)} = 1.03$ eV ($\lambda_{\mathrm{co}}^{(2)} = 1\,200$ nm) reduces the trimer lifetime to (400 ± 60) fs and for the deuterated trimer to (1.4 ± 0.3) ps. The corresponding photoelectron spectra reflect the energetics of the excitation as well as the ionization process and indicate cluster size-dependent shifts, *e.g.* of the

adiabatic ionization potentials. Moreover, the PES facilitate the identification of different signal contributions, *i.e.* nonresonant ionization, dissociative ionization and two-control photon absorption.

In contrast to the ammonia dimer, for which a crossing with a repulsive higher electronic state has been identified as decay mechanism [28], the present experimental findings can be explained consistently by assuming that for $m > 2$ an internal conversion back to the lowest $(NH_3)_{m-2}NH_4(3s)NH_2$ H-transfer state occurs, followed by fast dissociation. In particular, the lifetime dependence on the cluster size, deuteration and on excitation energy as well as the observed low-energy photoelectron peaks in the PES, corresponding to high vibrational energies in the photoions, corroborate this tentative assignment. Very similar observations for the isoelectronic system $Na(NH_3)_m$ indicate that the same fundamental mechanism is operative there too. Together, these results constitute a major challenge for a thorough theoretical investigation on this fundamental model process.

Financial support by the Deutsche Forschungsgemeinschaft through Sonderforschungsbereich 450, Teilprojekt A4, is gratefully acknowledged.

References

1. K.P. Sagarik, R. Ahlrichs, S. Brode, Mol. Phys. **57**, 1247 (1986).
2. J.C. Greer, R. Ahlrichs, I.V. Hertel, Z. Phys. D **18**, 413 (1991).
3. A. Tachibana, T. Suzuki, N. Yoshida, Y. Teramoto, T. Yamabe, Chem. Phys. **156**, 79 (1991).
4. H. Tachikawa, S. Tomoda, Chem. Phys. **182**, 185 (1994).
5. H. Tachikawa, Chem. Phys. **211**, 305 (1996).
6. N.B. Amor, D. Maynau, F. Spiegelmann, J. Chem. Phys. **104**, 4049 (1996).
7. J.K. Park, S. Iwata, J. Phys. Chem. A **101**, 3613 (1997).
8. S.T. Ceyer, P.W. Tiedemann, B.H. Mahan, Y.T. Lee, J. Chem. Phys. **70**, 14 (1979).
9. K. Stephan, J.H. Futrell, K.I. Peterson, A.W. Castleman Jr, H.E. Wagner, N. Djuric, T.D. Märk, Int. J. Mass Spectrom. Ion Phys. **44**, 167 (1982).
10. H. Shinohara, N. Nishi, N.J. Washida, J. Chem. Phys. **83**, 1939 (1985).
11. O. Echt, P.D. Dao, S. Morgan, A.W. Castleman Jr, J. Chem. Phys. **82**, 4076 (1985).
12. W. Kamke, B. Kamke, W. Wang, R. Hermann, I.V. Hertel, in *Physics and Chemistry of Small Clusters* (Plenum, New York, 1987), pp. 675-680.
13. W. Kamke, R. Hermann, W. Wang, I.V. Hertel, Z. Phys. D **10**, 491 (1988).
14. E. Kaiser, J. de Vries, H. Steger, C. Menzel, W. Kamke, I.V. Hertel, Z. Phys. D **20**, 193 (1991).
15. K. Fuke, R. Takasu, F. Misaizu, Chem. Phys. Lett. **229**, 597 (1994).
16. S. Wei, J. Purnell, S.A. Buzza, R.J. Stanley, A.W. Castleman Jr, J. Chem. Phys. **97**, 9480 (1992).
17. J. Purnell, S. Wei, S.A. Buzza, A.W. Castleman, J. Phys. Chem. **97**, 12530 (1993).
18. S.A. Buzza, S. Wei, J. Purnell, A.W. Castleman Jr, J. Chem. Phys. **102**, 4832 (1995).
19. T. Freudenberg, W. Radloff, H.-H. Ritze, V. Stert, F. Noack, I.V. Hertel, in *Femtochemistry*, edited by M. Chergui (World Scientific, Singapore, 1996), p. 255.
20. K. Fuke, R. Takasu, Bull. Chem. Soc. Jpn **68**, 3309 (1995).
21. T. Freudenberg, W. Radloff, H.-H. Ritze, V. Stert, K. Weyers, F. Noack, I.V. Hertel, Z. Phys. D **36**, 349 (1996).
22. T. Freudenberg, W. Radloff, H.-H. Ritze, V. Stert, F. Noack, I.V. Hertel, Z. Phys. D **41**, 267 (1997).
23. T. Freudenberg, V. Stert, W. Radloff, J. Ringling, J. Güdde, I.V. Hertel, Chem. Phys. Lett. **269**, 523 (1997).
24. V. Stert, W. Radloff, P. Farmanara, H.-H. Ritze, I.V. Hertel, in *Ultrafast Phenomena*, edited by T. Elsaesser, J.G. Fujimoto, D.A. Wiersma, W. Zinth (Springer Verlag, Heidelberg, 1998), p. 479.
25. P. Farmanara, W. Radloff, V. Stert, H.-H. Ritze, I.V. Hertel, J. Chem. Phys. **111**, 633 (1999).
26. W. Radloff, in *Photoionization and Photodetachment*, edited by C.-Y. Ng (World Scientific, Singapore, 2000), p. 127.
27. P. Farmanara, H.-H. Ritze, V. Stert, W. Radloff, I.V. Hertel, J. Chem. Phys. **115**, 277 (2001).
28. P. Farmanara, H.-H. Ritze, V. Stert, W. Radloff, I.V. Hertel, J. Chem. Phys. **116**, 1443 (2002).
29. J. Ringling, O. Kittelmann, F. Noack, G. Korn, J. Squier, Opt. Lett. **18**, 2035 (1993).
30. V. Stert, W. Radloff, T. Freudenberg, F. Noack, I.V. Hertel, C. Jouvet, C. Dedonder-Lardeux, D. Solgadi, Europhys. Lett. **40**, 515 (1997).
31. V. Stert, W. Radloff, C.-P. Schulz, I.V. Hertel, Eur. Phys. J. D **5**, 97 (1999).
32. W. Dohmke, G. Stock, Adv. Chem. Phys. **100**, 1 (1997).
33. C. Silva, P.K. Walhout, K. Yokoyama, P.F. Barbara, Phys. Rev. Lett. **80**, 1086 (1998).
34. W. Siebrand, J. Chem. Phys. **44**, 4055 (1966).
35. R. Englemen, J. Jortner, Mol. Phys. **18**, 145 (1970).
36. C.P. Schulz, A. Scholz, I.V. Hertel, in *Ultrafast Phenomena*, edited by T. Elsaesser, J.G. Fujimoto, D.A. Wiersma, W. Zinth (Springer Verlag, Heidelberg, 1998), p. 621.
37. A. Scholz, C.P. Schulz, I.V. Hertel, to be published.